The effect of composite material on Rayleigh wave at free surface of composite matrix saturated by fluids.

Ashish Arora[1] and Neeru Bala[2]

[1] Department of Mathematical Sciences, IKG Punjab Technical University, Kapurthala-144 603, Punjab, India.

[2]Department of Mathematics, DAV Institute of Engineering and Technology, Jalandhar-144 008, India

E-mail(s): dr.ashish10@hotmail, neeru.daviet@gmail.com

Abstract

The present study signifies the effect of distinct solids on the phase speed and attenuation of Rayleigh surface wave propagating on the boundary of composite porous matrix saturated with fluids. Secular equation depicting propagation of Rayleigh wave is obtained and solved numerically for obtaining phase speed and attenuation coefficient. Two different types of composite materials are considered for numerical study to analyze the effect of solids present in the structure. The study depicts that increase in rigidity of the composite increases the phase speed of the Rayleigh surface wave. Significant effect of the density and bulk modulus of fluid mixture present in the pores is also observed on the phase speed of the wave. The effect of porosity on the phase speed of the Rayleigh wave and the particle motion during the propagation of the wave is also analyzed.

Keywords: Composite porous medium; Rayleigh wave; Distinct solids, Phase speed, Attenuation; Porosity.

1 Introduction

The study of surface waves along the free interface is interesting and important due to its practical applicability in geotechnical studies, non-destructive testing, and crustal seismology. This study is gaining importance due to the increasing demand for efficient methodologies to apply in seismic engineering and geophysical exploration. The conventional methods of near surface geotechnical site investigation are not only localized and

Published by EDP Sciences and available at https://www.mmnp-journal.org or https://doi.org/10.1051/mmnp/2022025

time consuming but very costly. The Multichannel Analysis of Surface Waves (MASW) is an alternate non-invasive technique in geotechnical investigations (Tokeshi et al. 2013) and monitoring the properties of subsurface soil (Lu., 2014). The applications of the study of surface waves have been comprehensively studied by Moro (2015), Foti et al. (2015), Yilmaz (2015), and Ebrahimi (2018). The articles by Nenadic et al. (2011) and Colombi et al. (2016) are worth reading to understand the versatile applications of the study of surface waves. Nenadic et al. (2011) derived an algebraic relationship between the shear wave and Rayleigh wave velocity of a plate submerged in a fluid and applied the relationship to quantify mechanical properties of the heart wall and arteries. Colombi et al. (2016) have studied metamaterials that induce negative refraction for controlling the propagation of the Rayleigh wave.

The objective of the present formulation is to signify the effect of composite structure on the Rayleigh type surface wave propagating at the free boundary of a composite porous structure containing fluids. The fundamental study regarding the propagation of Rayleigh wave at porous medium has been conducted by Jones (1961), Deresiewicz (1962), Borcherdt (1973), Currie et al. (1977), Currie and O'Leary (1978), Currie (1979), Carcione (1992), Albers (2006) and Lo (2008). The effect of the structure of the medium and various material parameters on the propagation of the Rayleigh wave is an important part of academic studies as it is linked directly with real geotechnical problems. Vinh et al. (2016) derived a secular equation to study Rayleigh wave propagation in orthotropic fluid-saturated porous media. The authors depicted the strong effect of porosity and the elastic constants on the Rayleigh wave velocity. Gupta and Ahmed (2017) studied the Rayleigh wave propagation in pre-stressed orthotropic earth's crust over a transversely isotropic dissipative semi-infinite medium. The authors analyzed the effect of layer thickness, the presence of pre-stress, and corrugated surface on the phase velocity of the Rayleigh wave. Singh et al. (2018) studied the effect of various parameters like homogeneity, initial stress, wave number, and damping factor on Rayleigh wave propagating in incompressible viscoelastic media. Kumari et al. (2019) analyzed the impact of the corrugated interface on the phase speed and attenuation of the Rayleigh wave propagating on the surface of

micropolar porous half-space lying under a non-viscous liquid layer. Recently, Sharma (2020) has derived an explicit dispersion equation for the propagation of the Rayleigh wave in an orthotropic medium in the presence of initial stress and gravity and analyzed the effect on velocity and polarization of the Rayleigh wave.

The present formulation analyzes the effect of solids in the structure of composite porous material containing fluids, on the phase velocity and attenuation of the Rayleigh wave propagating on the surface of such medium. Painuley and Arora (2019) studied the propagation of the Rayleigh wave on the stress free boundary of the porous medium composed of two solids and saturated by two immiscible fluids. They borrowed the field equations developed by Arora et al. (2015) which are based upon Biot's theory. They analyzed the effect of saturation of fluids and porosity on the behavior of the Rayleigh wave. But the present study is based upon the mixture theory and signifies the effect of the presence of two different solids in the medium on the velocity and attenuation of the Rayleigh wave. To analyze the effect of rigidity of the solid matrix, two distinct composite structures are considered for the numerical study. In first case, the porous matrix is assumed to be formed of sand-ice and in second case the ice is replaced with clay. The pores of the matrix in both cases are assumed to be saturated with water and oil. The effect of porosity is also studied on the particle motion of the medium during the propagation of the Rayleigh wave.

2 Governing equations

We consider a composite porous medium composed of two distinct solids and saturated by two chemically non-reactive, immiscible fluids.The governing equations for such medium have been developed by generalizing the momentum balance equation in an Eulerian framework [Arora et al. 2016]. Under isothermal conditions and absence of body forces, these model equations are given by

$$\Big(A\frac{\partial^2}{\partial t^2} + B\frac{\partial}{\partial t}\Big)\mathrm{U} = N, \tag{1}$$

where

$$A = \begin{bmatrix} \rho_{s_1}\theta_{s_1} - \mathbb{A} & \mathbb{B} & \mathbb{C} & \mathbb{D} \\ \mathbb{B} & \rho_1\theta_1 - \mathbb{E} & -4A_{12} & \mathbb{B} \\ \mathbb{C} & -4A_{12} & \rho_2\theta_2 - \mathbb{F} & \mathbb{C} \\ \mathbb{D} & \mathbb{B} & \mathbb{C} & \rho_{s_2}\theta_{s_2} - \mathbb{A} \end{bmatrix}, \; B = \begin{bmatrix} -\mathbb{R} & R_{11} & R_{22} & 0 \\ R_{11} & -2R_{11} & 0 & R_{11} \\ R_{22} & 0 & -2R_{22} & R_{22} \\ 0 & R_{11} & R_{22} & -\mathbb{R} \end{bmatrix},$$

$$\mathrm{U} = \begin{bmatrix} \boldsymbol{u}_{s_1} \\ \boldsymbol{u}_1 \\ \boldsymbol{u}_2 \\ \boldsymbol{u}_{s_2} \end{bmatrix}, \quad \mathrm{N} = \begin{bmatrix} \nabla \cdot \sigma^{s_1} \\ \nabla \sigma^1 \\ \nabla \sigma^2 \\ \nabla \cdot \sigma^{s_2} \end{bmatrix}.$$

$\mathbb{A} = A_{11} + 2A_{12} + A_{22}, \quad \mathbb{B} = A_{11} + 2A_{12} + B_{11},$

$\mathbb{C} = A_{22} + 2A_{12} + B_{22}, \quad \mathbb{D} = -(B_{11} + 2A_{12} + B_{22}),$

$\mathbb{E} = 2(A_{11} + B_{11}), \quad \mathbb{F} = 2(A_{22} + B_{22}), \;\; \mathbb{R} = R_{11} + R_{22}.$

Solid and fluid phases in the composite porous matrix are represented by indices $s_1,\ s_2$ and $1,\ 2$, respectively. The symbols ρ_α, θ_α and $\boldsymbol{u_\alpha}$, $(\alpha = s_1, 1, 2, s_2)$ correspond to density, volume fraction and displacement field of each phase, respectively. The tensors σ^{s_1}, σ^{s_2} represent the components of stress on each solid phase and σ^1, σ^2 correspond to normal pressures on fluid phases. $R_{\gamma\beta}, \{(\gamma = 1, 2), (\gamma = \beta)\}$ symbolize the dissipation coefficients due to viscous drag where as $A_{\gamma\beta},\ (\gamma = \beta)$ correspond to inertial drag coefficients of first solid with first and second fluids. Similarly inertial drag coefficients for second solid are represented by $B_{\gamma\beta}$. Cross coupling between fluid phases is assumed to be symmetric and denoted by $A_{\gamma\beta} = B_{\gamma\beta}, (\gamma \neq \beta)$. The expressions of viscous and inertial drag coefficients are given in Appendix.

The fluid pressures $p_1,\ p_2$ and the dilatational stresses p_{s_1} and p_{s_2} in terms of porosity change can be expressed as

$$\begin{aligned} \frac{\partial p_{s_\gamma}}{\partial t} &= -K_{s_\gamma} \nabla \cdot V_{s_\gamma} + \frac{K_{s_\gamma}}{1-\phi} \frac{\partial \phi}{\partial t} \\ \frac{\partial p_\gamma}{\partial t} &= -K_\gamma \nabla \cdot V_\gamma - \frac{K_\gamma}{\phi} \frac{\partial \phi}{\partial t} - \frac{K_\gamma}{S_\gamma} \frac{\partial S_\gamma}{\partial t}. \end{aligned} \tag{2}$$

The fluid saturation is given by $S_\gamma = \dfrac{\theta_\gamma}{\phi}$, where ϕ is the porosity of the medium. The relationship of the porosity change with the dilatation of the fluid and solid phases may

be expressed as

$$\frac{\partial \phi}{\partial t} = \sum \delta_\alpha \nabla \cdot V_\alpha, \tag{3}$$

where δ_α are the dimensionless parameters. To find the expressions of these parameters, we use the conditions of generalized jacketed and un-jacketed compressibility tests. In the jacketed test, a sample of the porous medium is enclosed in a thin impermeable jacket. The fluids present in the sample are given outlets through the tubes T_1 and T_2. The tube T_1 is permeable to the first fluid, while the tube T_2 is permeable to the second fluid. Both the tubes are connected to corresponding containers filled with the first and second fluids kept at the reference pressures p_1 and p_2, respectively. External pressure is then applied to the sample. During this process, the fluid pressures in the sample remain unaltered due to outlets T_1 and T_2, and the whole pressure is therefore exerted on the drained solid matrix. The mathematical conditions for this experiment can be expressed as

$$\frac{\partial p_f}{\partial t} = 0; \quad e^{(s_\gamma)} = \frac{\theta_{s_\gamma}}{K'_{s_\gamma}} p_{s_\gamma}. \tag{4}$$

Here, the symbol $p_f = S_1 p_1 + (1 - S_1) p_2$ stands for the average fluid pressure. The dilatation in the solid phase is represented by $e^{(s_\gamma)} (= \nabla \cdot \mathbf{u}_{s_\gamma})$ and the symbol K'_{s_γ} represents bulk modulus of the drained solid.

In the un-jacketed experiment, the sample of the medium is immersed in a mixture of the first and second fluid. The proportion of both the fluids in the mixture is kept the same as in the pores of the sample. A uniformly distributed external pressure is applied in the fluid mixture, such that the average fluid pressure p_f becomes equal to the mean dilatational principal stress p_s on the solid frame. The porosity of the sample remains unchanged throughout the process. The conditions for generalized un-jacketed experiment can be expressed as

$$p_s = p_f; \quad \frac{\partial \phi}{\partial t} = 0. \tag{5}$$

employing (4)-(5) in the closure relation of porosity change (3), we obtain the expressions of the dimensionless parameters δ_α. The expressions of these parameters are given in

Appendix. Employing (3) and the relation $\dfrac{\partial S_1}{\partial t} = \dfrac{dS_1}{dp_c}\left(\dfrac{\partial p_1}{\partial t} - \dfrac{\partial p_2}{\partial t}\right)$ in (2), we obtain the following stress-strain relations.

$$-S_{s_1}\theta_s \frac{\partial p_{s_1}}{\partial t} = \nabla \cdot (a_{11}V_{s_1} + a_{12}V_1 + a_{13}V_2 + a_{14}V_{s_2}), \tag{6}$$

$$-\phi S_1 \frac{\partial p_1}{\partial t} = \nabla \cdot (a_{12}V_{s_1} + a_{22}V_1 + a_{23}V_2 + a_{24}V_{s_2}), \tag{7}$$

$$-\phi S_2 \frac{\partial p_2}{\partial t} = \nabla \cdot (a_{13}V_{s_1} + a_{23}V_1 + a_{33}V_2 + a_{34}V_{s_2}), \tag{8}$$

$$-S_{s_2}\theta_2 \frac{\partial p_{s_2}}{\partial t} = \nabla \cdot (a_{14}V_{s_1} + a_{24}V_1 + a_{34}V_2 + a_{44}V_{s_2}), \tag{9}$$

where the expressions of the coefficients are incorporated in the Appendix. The stress tensor on each solid phase can be expressed as

$$t_{s_\gamma} = -\theta_{s_\gamma} p_{s_\gamma} I + 2G_{s_\gamma}\mathbf{e}_{s_\gamma} - \frac{2}{3}G_{s_\gamma}\nabla \cdot \mathbf{u}_{s_\gamma} I, \tag{10}$$

where I is a unit tensor matrix and $\mathbf{e}_{s_\gamma} = \frac{1}{2}(\nabla \mathbf{u}_{s_\gamma} + \nabla \mathbf{u}_{s_\gamma}^T)$ represents the dilatation of the solid phase. Integrating equations (6)-(9) by keeping $\phi,\ S_1, S_{s_1},\ a_{ij}$ fixed, and using (10), we obtain the following linear constitutive relations for the medium.

$$\sigma^{s_1} = [(a_{11} - \frac{2}{3}G_{s_1})\nabla \cdot \mathbf{u}_{s_1} + a_{12}\nabla \cdot \mathbf{u}_1 + a_{13}\nabla \cdot \mathbf{u}_2 + a_{14}\nabla \cdot \mathbf{u}_{s_2}]I + 2G_{s_1}(\mathbf{e_{s_1}}), \tag{11}$$

$$\sigma^{s_2} = (a_{14}\nabla \cdot \mathbf{u}_{s_1} + a_{24}\nabla \cdot \mathbf{u}_1 + a_{34}\nabla \cdot \mathbf{u}_2 + (a_{44} - \frac{2}{3}G_{s_2})\nabla \cdot \mathbf{u}_{s_2})I + 2G_{s_2}(\mathbf{e_{s_2}}), \tag{12}$$

$$\sigma^1 = (a_{12}\nabla \cdot \mathbf{u}_{s_1} + a_{22}\nabla \cdot \mathbf{u}_1 + a_{23}\nabla \cdot \mathbf{u}_2 + a_{24}\nabla \cdot \mathbf{u}_{s_2})I, \tag{13}$$

$$\sigma^2 = (a_{13}\nabla \cdot \mathbf{u}_{s_1} + a_{23}\nabla \cdot \mathbf{u}_1 + a_{33}\nabla \cdot \mathbf{u}_2 + a_{34}\nabla \cdot \mathbf{u}_{s_2})I. \tag{14}$$

For the propagation of plane dilatational and rotational wave in the medium, we consider the displacement vector in terms of scalar and vector potential by using Helmholtz representation as follows

$$\mathbf{u}_\alpha = (\nabla \bar{\phi_\alpha} + \nabla \times \bar{\boldsymbol{\psi}}_\alpha)\exp^{-\iota\omega t}, \tag{15}$$

where the scalar potential $\bar{\phi_\alpha}$ corresponds to dilatation in the medium and the vector potential $\bar{\boldsymbol{\psi}}_\alpha$ depicts the distortion in the medium. The symbol ω represents angular frequency. Employing the relation (15) in (1), the general field equations are split into

following two sets of four differential equations.

$$\begin{aligned} L_1\bar{\Phi} &= \mathcal{O}, \\ L_2\bar{\Psi} &= \mathcal{O}, \end{aligned} \tag{16}$$

where

$$L_1 = \begin{pmatrix} \bar{a}_{11}\mathrm{Y}+\eta_{00} & a_{12}\mathrm{Y}+\eta_{01} & a_{13}\mathrm{Y}+\eta_{02} & a_{14}\mathrm{Y}+\eta_{03} \\ a_{12}\mathrm{Y}+\eta_{01} & a_{22}\mathrm{Y}+\eta_{11} & a_{23}\mathrm{Y}+\eta_{12} & a_{24}\mathrm{Y}+\eta_{01} \\ a_{13}\mathrm{Y}+\eta_{02} & a_{23}\mathrm{Y}+\eta_{12} & a_{33}\mathrm{Y}+\eta_{23} & a_{34}\mathrm{Y}+\eta_{02} \\ a_{14}\mathrm{Y}+\eta_{03} & a_{24}\mathrm{Y}+\eta_{01} & a_{34}\mathrm{Y}+\eta_{02} & \bar{a}_{44}\mathrm{Y}+\eta_{44} \end{pmatrix},$$

$$L_2 = \begin{pmatrix} G_{s_1}\mathrm{Y}+\eta_{00} & \eta_{01} & \eta_{02} & \eta_{03} \\ \eta_{01} & \eta_{11} & \eta_{12} & \eta_{01} \\ \eta_{02} & \eta_{12} & \eta_{23} & \eta_{02} \\ \eta_{03} & \eta_{01} & \eta_{02} & G_{s_2}\mathrm{Y}+\eta_{44} \end{pmatrix}, \qquad \mathrm{Y} = \frac{\nabla^2}{\omega^2},$$

and $\mathcal{O}$ represents the null matrix. The expressions of other symbols are given as

$\bar{\Phi} = [\bar{\phi_{s_1}}\ \bar{\phi_1}\ \bar{\phi_2}\ \bar{\phi_{s_2}}]^T$, $\bar{\Psi} = [\bar{\boldsymbol{\psi}_{s_1}}\ \bar{\boldsymbol{\psi}_1}\ \bar{\boldsymbol{\psi}_2}\ \bar{\boldsymbol{\psi}_{s_2}}]^T$,

$\bar{a}_{11} = a_{11} + \frac{4}{3}G_{s_1}$, $\bar{a}_{44} = a_{44} + \frac{4}{3}G_{s_2}$, $\eta_{00} = \rho_{s_1}\theta_{s_1} - \mathbb{A} - \frac{\iota}{\omega}\mathbb{R}$,

$\eta_{44} = \rho_{s_2}\theta_{s_2} - \mathbb{A} - \frac{\iota}{\omega}\mathbb{R}$, $\eta_{03} = -(B_{11} + B_{22} + 2A_{12})$,

$\eta_{01} = A_{11} + 2A_{12} + B_{11} + \frac{\iota}{\omega}R_{11}$, $\eta_{02} = A_{22} + 2A_{12} + B_{22} + \frac{\iota}{\omega}R_{22}$,

$\eta_{11} = \rho_1\theta_1 - 2(A_{11} + B_{11}) - 2\frac{\iota}{\omega}R_{11}$, $\eta_{12} = -4A_{12}$,

$\eta_{23} = \rho_2\theta_2 - 2(A_{22} + B_{22}) - 2\frac{\iota}{\omega}R_{22}$.

Using last three rows of the matrix representation given by (16) and applying crammers rule, we obtain

$$(\bar{\phi_1} : \bar{\phi_2} : \bar{\phi_{s_2}} : \bar{\phi_{s_1}}) = \ell_1 : \ell_2 : \ell_3 : \ell_4, \tag{17}$$

$$(\bar{\boldsymbol{\psi}_1} : \bar{\boldsymbol{\psi}_2} : \bar{\boldsymbol{\psi}_{s_2}} : \bar{\boldsymbol{\psi}_{s_1}}) = \epsilon_1 : \epsilon_2 : \epsilon_3 : \epsilon_4, \tag{18}$$

where the expressions of various symbols defined above are given in Appendix. Employing these relations in the first row of (16), we can write

$$|L_1|\bar{\phi_{s_1}} = 0 = |L_2|\bar{\psi_{s_1}}, \tag{19}$$

where symbol (||) stands for the determinant. This gives the following partial differential equations representing the propagation of dilatational and rotational waves, respectively.

$$(\nabla^2 + k_1^2)(\nabla^2 + k_2^2)(\nabla^2 + k_3^2)(\nabla^2 + k_4^2)\bar{\phi_{s_1}} = 0, \tag{20}$$

$$(\nabla^2 + k_5^2)(\nabla^2 + k_6^2)\bar{\boldsymbol{\psi}_{\boldsymbol{s_1}}} = 0. \tag{21}$$

The general solutions of (20) and (21) may be written as

$$(\bar{\phi_{s_1}}, \quad \bar{\boldsymbol{\psi}_{s_1}}) = \left(\sum_{\beta=1}^{4} \phi^{\beta}, \quad \sum_{l=5}^{6} \boldsymbol{\psi^l} \right), \tag{22}$$

where ϕ^{β} and $\boldsymbol{\psi^l}$ satisfy the Helmholtz equations

$$(\nabla^2 + k_{\beta}^2)\phi^{\beta} = 0, \quad (\nabla^2 + k_l^2)\boldsymbol{\psi^l} = 0. \tag{23}$$

The symbols k_{β} and k_l correspond to complex wavenumbers of dilatational and shear waves, respectively. This reveals the existence of six waves in the medium. The four, out of these six waves are dilatational in nature, while two are shear in nature. The dilatational waves may be designated by $P_{\beta}, (\beta = 1, 2, 3, 4)$ and the shear waves by $S_l, (l = 5, 6)$. For physically meaningful solution the imaginary part of complex wave number k_{β}, k_l are chosen to be positive. Using (17)-(18) and (22), we get the following coupling relations

$$\bar{\phi_{\alpha}} = \lambda_{\alpha}^{\beta}\phi^{\beta}, \quad \bar{\boldsymbol{\psi}}_{\alpha} = \lambda_{\alpha}^{l}\boldsymbol{\psi}^{l}, \tag{24}$$

where summation convention is used over the repeated index. The expressions of coefficients of coupling relations are also incorporated in the Appendix.

3 Secular equation

We consider an infinite half-space composed of two distinct solids and containing two immiscible fluids occupying a region $z \geq 0$ in the rectangular coordinate system O_{xyz}. Due to the uniformity of an isotropic system in all directions, the two dimensional case

can be generalized to three dimensional case. Therefore, we consider a two dimensional case in xz-plane, where $z = 0$ represents the free surface of the medium. As revealed in the previous section, six coupled waves propagate in such a medium. The four waves, among these six waves, are dilatational and two are shear in nature. The displacement in each phase is the resultant of all dilatational and distortional displacements caused by the body waves. Therefore, we can write

$$\mathbf{u}_\alpha = (u_{\alpha x}, 0, u_{\alpha z}) = \sum_{\beta=1}^{4} \lambda_\alpha^\beta \nabla \phi^\beta + \sum_{l=5}^{6} \lambda_\alpha^l \nabla \times \boldsymbol{\psi}^l. \tag{25}$$

Consider the propagation of Rayleigh surface wave along the free surface of the medium and decaying exponentially along z-direction. The displacement potentials representing the propagation of Rayleigh wave are given by

$$\phi^\beta = A_\beta \exp(-b_\beta z) \exp \iota(k_r x - \omega t), \quad \phi^l = A_l \exp(-b_l z) \exp \iota(k_r x - \omega t), \tag{26}$$

where $b_\beta = \sqrt{(k_r^2 - k_\beta^2)}, \quad b_l = \sqrt{(k_r^2 - k_l^2)}$.

The symbols ϕ^5 and ϕ^6, respectively represent y-component of vectors $\boldsymbol{\psi}^5$ and $\boldsymbol{\psi}^6$. The symbol $k_r (= \Re(k_r) + \iota \Im(k_r))$ represents the complex wave number of the Rayleigh wave, where $\Re()$ and $\Im()$ are the real and imaginary parts of a complex quantity. It is considered that $\Re(k_r) \geq 0$. This is to ensure the propagation of Rayleigh wave in positive x-direction. Since the quantities $b_m, (m = 1, 2...6)$ are complex valued, therefore to ensure the attenuation of wave in positive z-direction, we consider $\Re(b_m) \geq 0$. The boundary of composite porous medium $z = 0$ is assumed to be flat and mechanically stress free. Therefore, we consider normal stress σ_{zz}, tangential stress σ_{zx} and the fluid pressure σ to be zero at the surface $z = 0$. Mathematically, we can write these conditions as follows

$$\begin{aligned} &(i)\ \sigma_{zz}^{s_1} = 0, \quad (ii)\ \sigma_{zx}^{s_1} = 0, \quad (iii)\ \sigma^1 = 0 \\ &(iv)\ \sigma^2 = 0, \quad (v)\ \sigma_{zz}^{s_2} = 0, \quad (vi)\ \sigma_{zx}^{s_2} = 0. \end{aligned} \tag{27}$$

Using (25), (26) and the constitutive relations (11)-(14) in above boundary conditions, we obtain following six linear equations in A_m, $m = 1, 2...6$.

$$\sum_{\beta=1}^{4} (2G_{s_1} {k_r}^2 - r_\beta k_\beta^2) A_\beta - \sum_{l=5}^{6} \mathcal{Q}_1 \sqrt{(k_r^2 - k_l^2)} A_l k_r = 0, \tag{28}$$

$$\sum_{\beta=1}^{4} -\mathcal{Q}_1\sqrt{(k_r^2-k_\beta^2)}A_\beta k_r - \sum_{l=5}^{6} G_{s_1}(2k_r^2-k_l^2)A_l = 0, \tag{29}$$

$$\sum_{\beta=1}^{4} \varpi_\beta k_\beta^2 A_\beta = 0, \quad \sum_{\beta=1}^{4} \zeta_\beta k_\beta^2 A_\beta = 0, \tag{30}$$

$$\sum_{\beta=1}^{4} (2G_{s_2}\lambda_{s_2}^\beta {k_r}^2 - \mathfrak{s}_\beta k_\beta^2)A_\beta - \sum_{l=5}^{6} \mathcal{P}_l\sqrt{(k_r^2-k_l^2)}A_l k_r = 0, \tag{31}$$

$$\sum_{\beta=1}^{4} \mathcal{P}_\beta\sqrt{(k_r^2-k_\beta^2)}A_\beta k_r - \sum_{l=5}^{6} G_{s_2}\lambda_{s_2}^l(2k_r^2-k_l^2)A_l = 0, \tag{32}$$

where

$r_\beta = J_\beta + 2G_{s_1}$, $\mathcal{Q}_1 = 2\iota G_{s_1}$, $\varpi_\beta = a_{12} + \lambda_1^\beta a_{22} + \lambda_2^\beta a_{23} + \lambda_{s_2}^\beta a_{24}$,

$\zeta_\beta = a_{13} + \lambda_1^\beta a_{23} + \lambda_2^\beta a_{33} + \lambda_{s_2}^\beta a_{34}$, $\mathfrak{s}_\beta = \mathcal{M}_\beta + 2G_{s_2}\lambda_{s_2}^\beta$,

$J_\beta = (a_{11} - \frac{2}{3}G_{s_1} + a_{12}\lambda_1^\beta + a_{13}\lambda_2^\beta + a_{14}\lambda_{s_2}^\beta)$,

$\mathcal{M}_\beta = a_{14} + a_{24}\lambda_1^\beta + a_{34}\lambda_2^\beta + (a_{44} - \frac{2}{3}G_{s_2})\lambda_{s_2}^\beta$,

$\mathcal{P}_\beta = -2\iota G_{s_2}\lambda_{s_2}^\beta$, $\mathcal{P}_l = 2\iota G_{s_2}\lambda_{s_2}^l$.

Non trivial solution of this system of equations leads to an irrational equation in k_r. The frequency equation can be obtained by taking the determinant of the coefficient matrix equal to zero as given below

$$\begin{vmatrix}
2G_{s_1} - r_1\frac{k_1^2}{k_r^2} & 2G_{s_1} - r_2\frac{k_2^2}{k_r^2} & 2G_{s_1} - r_3\frac{k_3^2}{k_r^2} & 2G_{s_1} - r_4\frac{k_4^2}{k_r^2} & -\mathcal{Q}_1\mathfrak{d}_5 & -\mathcal{Q}_1\mathfrak{d}_6 \\
-\mathcal{Q}_1\mathfrak{d}_1 & -\mathcal{Q}_1\mathfrak{d}_2 & -\mathcal{Q}_1\mathfrak{d}_3 & -\mathcal{Q}_1\mathfrak{d}_4 & -G_{s_1}\mathfrak{t}_5 & -G_{s_1}\mathfrak{t}_6 \\
\varpi_1 k_1^2 & \varpi_2 k_2^2 & \varpi_3 k_3^2 & \varpi_4 k_4^2 & 0 & 0 \\
\zeta_1 k_1^2 & \zeta_2 k_2^2 & \zeta_3 k_3^2 & \zeta_4 k_4^2 & 0 & 0 \\
2G_{s_2}\lambda_{s_2}^1 - \mathfrak{s}_1\frac{k_1^2}{k_r^2} & 2G_{s_2}\lambda_{s_2}^2 - \mathfrak{s}_2\frac{k_2^2}{k_r^2} & 2G_{s_2}\lambda_{s_2}^3 - \mathfrak{s}_3\frac{k_3^2}{k_r^2} & 2G_{s_2}\lambda_{s_2}^4 - \mathfrak{s}_4\frac{k_4^2}{k_r^2} & -\mathcal{P}_5\mathfrak{d}_5 & -\mathcal{P}_6\mathfrak{d}_6 \\
\mathcal{P}_1\mathfrak{d}_1 & \mathcal{P}_2\mathfrak{d}_2 & \mathcal{P}_3\mathfrak{d}_3 & \mathcal{P}_4\mathfrak{d}_4 & -G_{s_2}\lambda_{s_2}^5\mathfrak{t}_5 & -G_{s_2}\lambda_{s_2}^6\mathfrak{t}_6
\end{vmatrix} = 0, \tag{33}$$

where $\mathfrak{d}_m = \sqrt{\left(1 - \frac{k_m^2}{k_r^2}\right)}$, $\mathfrak{t}_l = \left(2 - \frac{k_l^2}{k_r^2}\right)$.

At stipulated wave frequency ω, the phase speed V_r and attenuation coefficient A_r of

Rayleigh wave are given by

$$V_r = \frac{\omega}{\Re(k_r)}, \qquad |A_r| = \Im(k_r). \tag{34}$$

We may reduce the secular equation (33) of Rayleigh wave to the corresponding secular equation of a Rayleigh wave propagating in a porous medium composed of a single solid and saturated by immiscible fluids. Our model equations are directly reducible to the model equations developed by Lo et al. (2005) for the porous medium composed of a single solid and saturated by two immiscible fluids by assuming $K_{s_2}, \theta_{s_2}, \rho_{s_2}$ and G_{s_2} all equal to zero (Arora et al. 2016). With this type of assumption three dilatational and one shear wave propagate through the medium. Also, in this manner, the equation (33) reduces to the following form.

$$\begin{vmatrix} -\mathcal{S}_1\dfrac{k_1^2}{k_r^2}+2G_{s_1} & -\mathcal{S}_2\dfrac{k_2^2}{k_r^2}+2G_{s_1} & -\mathcal{S}_3\dfrac{k_3^2}{k_r^2}+2G_{s_1} & -2\iota G_{s_1}\mathfrak{d}_5 \\ -2\iota G_{s_1}\mathfrak{d}_1 & -2\iota G_{s_1}\mathfrak{d}_2 & -2\iota G_{s_1}\mathfrak{d}_3 & -G_{s_1}\mathfrak{t}_5 \\ \mathcal{R}_1k_1^2 & \mathcal{R}_2k_2^2 & \mathcal{R}_3k_3^2 & 0 \\ \mathcal{A}_1k_1^2 & \mathcal{A}_2k_2^2 & \mathcal{A}_3k_3^2 & 0 \end{vmatrix} = 0, \tag{35}$$

where

$\mathcal{S}_\beta = (\bar{a}_{11} + a_{12}\lambda_1^\beta + a_{13}\lambda_2^\beta)$, $\mathcal{R}_\beta = (a_{12} + \lambda_1^\beta a_{22} + \lambda_2^\beta a_{23})$, $\mathcal{A}_\beta = (a_{13} + \lambda_1^\beta a_{23} + \lambda_2^\beta a_{33})$. The equation (35) can also be rewritten as follows

$$4\mathfrak{d}_5\sum_{\beta=1}^{3}\mathcal{E}_\beta\mathfrak{d}_\beta = (2-\mathrm{w})\Big(2\sum_{\beta=1}^{3}\mathcal{E}_\beta - \mathrm{w}\sum_{\beta=1}^{3}\mathcal{E}_\beta\mathcal{C}_\beta\Big), \quad \mathrm{w} = \frac{V_r^2}{v_5^2}, \tag{36}$$

where

$\mathcal{C}_\beta = \dfrac{\mathcal{S}_\beta\mathfrak{q}_\beta}{G_{s_1}}$, $\mathfrak{q}_\beta = \dfrac{v_5^2}{v_\beta^2}$, $\mathcal{E}_1 = \mathcal{G}_2\mathcal{H}_3 - \mathcal{H}_2\mathcal{G}_3$, $\mathcal{E}_2 = \mathcal{G}_3\mathcal{H}_1 - \mathcal{H}_3\mathcal{G}_1$, $\mathcal{E}_3 = \mathcal{G}_1\mathcal{H}_2 - \mathcal{H}_1\mathcal{G}_2$,

$\mathcal{G}_\beta = \dfrac{\mathcal{R}_\beta}{v_\beta^2}$, $\mathcal{H}_\beta = \dfrac{\mathcal{A}_\beta}{v_5^2}$.

The symbol v_β represents the phase speed of dilatational waves and v_5 denotes the phase speed of shear wave propagating in the medium. The equation (36) gives the frequency equation of Rayleigh wave propagating in a porous medium containing single solid and two immiscible fluids [Sharma (2012)].

Similarly, we may reduce the secular equation of the Rayleigh wave in the present medium to the corresponding secular equation of the Rayleigh wave propagating in an elastic solid by eliminating the parameters corresponding to one of the solids and both the fluids. We assume $\rho_1 = \theta_1 = K_1 = \rho_2 = \theta_2 = K_2 = 0$ and $K_{s_2} = \theta_{s_2} = \rho_{s_2} = G_{s_2} = 0$. Under these assumptions only one dilatational and one shear wave propagate in the medium. The frequency equation for a Rayleigh wave propagating in an elastic solid may be expressed as (Ewing and Jardetzky, 1957)

$$\begin{vmatrix} -\bar{a}_{11}\dfrac{k_1^2}{k_r^2} + 2G_{s_1} & -2\iota G_{s_1}\mathfrak{d}_5 \\ -2\iota G_{s_1}\mathfrak{d}_1 & -G_{s_1}\mathfrak{t}_5 \end{vmatrix} = 0 \tag{37}$$

The equation (37) can be rewritten in the following form

$$\mathfrak{t}_5^2 = 4\mathfrak{d}_1\mathfrak{d}_5,$$

where $v_1 = \sqrt{\dfrac{\bar{a}_{11}}{\rho_{s_1}}}$, $v_5 = \sqrt{\dfrac{G_{s_1}}{\rho_{s_1}}}$.

4 Particle motion in the medium

During the propagation of a wave, the oscillating particles of the medium trace a particular trajectory. In the present section, we study the trajectory traced out by the particle during the propagation of the Rayleigh surface wave in the medium. Using (25), the aggregate displacement $(U_x, 0, U_z)$ in the medium may be written as

$$U_x = u_{s_1 x} + u_{1x} + u_{2x} + u_{s_2 x} = \sum_{\beta=1}^{4} L^\beta \frac{\partial \phi^\beta}{\partial x} - \sum_{l=5}^{6} L^l \frac{\partial \phi^l}{\partial z}, \tag{38}$$

$$U_z = u_{s_1 z} + u_{1z} + u_{2z} + u_{s_2 z} = \sum_{\beta=1}^{4} L^\beta \frac{\partial \phi^\beta}{\partial z} + \sum_{l=5}^{6} L^l \frac{\partial \phi^l}{\partial x}, \tag{39}$$

where $L^\beta = \lambda_{s_1}^\beta + \lambda_1^\beta + \lambda_2^\beta + \lambda_{s_2}^\beta$, $\quad L^l = \lambda_{s_1}^l + \lambda_1^l + \lambda_2^l + \lambda_{s_2}^l$.

On inserting the expressions of potentials from (26) into (38)-(39), we get

$$\{U_x, 0, U_z\} = \{\iota|\nu_0| \exp^{\iota\Theta_1}, 0, -|\mu_0| \exp^{\iota\Theta_2}\} \exp[-\Im(k_r)x], \tag{40}$$

where

$$\nu_0 = k_r A_1 \Big[\sum_{\beta=1}^{4} L^\beta \frac{A_\beta}{A_1} \exp(-b_\beta z) - \iota \sum_{l=5}^{6} L^l \frac{A_l}{A_1} \frac{b_l}{k_r} \exp(-b_l z) \Big], \tag{41}$$

$$\mu_0 = k_r A_1 \Big[\sum_{\beta=1}^{4} L^\beta \frac{A_\beta}{A_1} \frac{b_\beta}{k_r} \exp(-b_\beta z) - \iota \sum_{l=5}^{6} L^l \frac{A_l}{A_1} \exp(-b_l z) \Big], \tag{42}$$

$\Theta_1 = \arg \nu_0 + \theta, \;\; \Theta_2 = \arg \mu_0 + \theta, \quad \theta = \Re(k_r)x - \omega t.$

The displacement of particles in medium for the Rayleigh surface wave are given by

$$r_x = \Re(U_x) = -|\nu_0| \sin \Theta_1 \exp[-\Im(k_r)x], \quad r_z = \Re(U_z) = -|\mu_0| \cos \Theta_2 \exp[-\Im(k_r)x]. \tag{43}$$

The unknown parameter θ assumes the values in $[0, 2\pi)$. From (43), we may get

$$C_1 r_x^2 - C_2 r_x r_z + C_3 r_z^2 = 1, \tag{44}$$

where

$$C_1 = \frac{1}{|\nu_0|^2 \exp[-\Im(k_r)x]^2 \cos^2(\xi)}, \quad C_2 = \frac{2 \sin(\xi)}{|\nu_0||\mu_0| \exp[-\Im(k_r)x]^2 \cos^2(\xi)},$$
$$C_3 = \frac{1}{|\mu_0|^2 \exp[-\Im(k_r)x]^2 \cos^2(\xi)}, \qquad \xi = \arg \nu_0 - \arg \mu_0.$$

The discriminant of (44) ($C_2^2 - 4C_1C_3 \leq 0$) indicates that during the propagation of Rayleigh surface wave, the particle traces an elliptical curve. In next section we shall also study the effect of material parameters on the elliptic curve traced out by the particle.

5 Numerical results and discussion

To study the behavior of the Rayleigh wave and its dependency upon various parameters of the medium, we compare the phase speed of the Rayleigh wave in different composite structures. In the first case, we consider the composite porous matrix composed of sand and ice. In the second case, we replace the ice with clay and compare the phase speed of the Rayleigh wave with the variation in sand fraction. The pores in both cases are assumed to be saturated with water and oil. The effect of variation in water is also studied on the phase speed of the Rayleigh wave in both cases of the composite matrix. This study

is applicable in subsurface hydrology and to study the strength of the material. The composite materials are being developed as construction material, and the propagation of a surface wave through such materials helps analyze their stability. For example, the sand-clay composite is used for the construction of lightweight material based upon vegetable fibers (Omrani et al. 2020). A mixture of clay (60%) and natural sand (40%) is reinforced with fibers extracted from Jancus acutus. The reinforced ice is also used as alternate construction material in cold regions. Various types of ice-soil reinforcement are formulated for the development of innovative materials (Nicolai et al. 2015). Moreover, most of the rocks are natural composite porous materials containing fluids. The Bulk modulus, porosity, permeability, and the density of various constituents of the material play important role in analyzing the strength of a material and helpful in understanding the structure. The effect of these parameters is studied in this section. Table-I gives the numerical values employed for the various parameters of the medium. (Leclaire et al. 1994; Lo et al. 2005).

Using the given parametric values the equations (20) and (21) are solved to find the wave numbers of dilatational and shear waves propagating in the medium. These values are substituted in (28)-(32) to obtain the set of six linear homogeneous equations in unknowns A_m. The condition for obtaining a non-trivial solution of this set of equations leads to an irrational equation in k_r. This equation contains six radical terms. For rationalizing, it requires successive squaring and rearranging of terms six times and hence produces extraneous roots. This process is also very difficult and the identification of original roots becomes very stiff. Therefore, we rely upon the iterative technique to solve this equation. The numerical solution of this equation yields a complex approximate value of wave number (k_r) of the Rayleigh wave propagating in the medium. Then the phase speed and attenuation coefficient of the Rayleigh wave are calculated by using (34). This type of wave is called a quasi-elastic wave. Although, some researchers (Currie et al. (1977), Romeo (2001)) have witnessed two distinct modes of Rayleigh surface waves, termed as quasi-elastic and visco-elastic waves traveling together. But as established by Sharma (2012), the viso-elastic Rayleigh wave appears only in viso-elastic media and for a given

Table-I: Values of parameters

Parameters	$Values$
Bulk modulus of Ice (K_{s_1})	8.5 Gpa
Bulk modulus of sand (K_{s_2})	35Gpa
Bulk modulus of Clay (K_{s_1})	20 Gpa
Bulk modulus of Oil (K_1)	0.57 Gpa
Bulk modulus of Water (K_2)	2.25 Gpa
Density of Ice (ρ_{s_1})	900 Kg/m^3
Density of sand (ρ_{s_2})	$2650Kg/m^3$
Density of Clay (ρ_{s_1})	2100 Kg/m^3
Density of Oil (ρ_1)	762 Kg/m^3
Density of Water (ρ_2)	1000 Kg/m^3
Drained bulk modulus of Ice ($K^d_{s_1}$)	250 Mpa
Drained bulk modulus of sand ($K^d_{s_2}$)	83.3 Mpa
Drained bulk modulus of Clay ($K^d_{s_1}$)	200 Mpa
Shear modulus of Ice (G_{s_1})	3.6 Gpa
Shear modulus of sand (G_{s_2})	3.85 Mpa
Shear modulus of Clay (G_{s_1})	3 Gpa
Permeability of Ice ($\mathbb{K}_{s_1}$)	0.0107 μm^2
Permeability of sand ($\mathbb{K}_{s_2}$)	0.8 Pico m^2
Permeability of Clay ($\mathbb{K}_{s_1}$)	0.00000107 μm^2
Viscosity of Oil (η_1)	14400 $\mu Ns/m^2$
Viscosity of Water (η_2)	.001 Ns/m^2
Porosity	0.50
i(Fitting parameter)	25×10^{-5}

frequency this wave exists only for certain range of complex values of Lame parameters. In poro-elastic media only quasi-elastic Rayleigh wave is visible. The single root of k_r corresponds to the wave number of the single Rayleigh wave traveling in the medium. Figures 1-2 depict the variation of phase speed (P_r) and attenuation coefficient (A_r) of a Rayleigh wave with angular frequency (ω) for both sand-ice and sand-clay composites. The graphs are shown at two distinct values of sand fraction in the composite porous matrix. The values of porosity (ϕ) and water saturation (S_2) in pores are considered to be 0.5. It is found that the phase speed of a Rayleigh wave increases with an increase in the angular frequency for both systems. It is noticeable from figure 1 that a decrease in sand

fraction increases the phase speed of the Rayleigh wave. This is attributed to the increase in ice content and hence increase in the permeability of the medium. The increase in permeability decreases the attenuation coefficient [Dia et al. (2006)]. This directly affects the phase speed of the Rayleigh surface wave. This fact is also evident from the sand-clay composite as shown in figure 2. The attenuation of both the P and S-waves increases in the given frequency range [Arora et al. (2016)] and hence the increase in attenuation in both the cases is observed in the frequency range under consideration. The phase speed of Rayleigh wave in sand-clay composite is much slower than that propagates in the sand-ice composite.

Figures 3-4 depict the variation in phase speed and attenuation coefficient of a Rayleigh surface wave with angular frequency at two different values of water saturation in pores of both the composite media. An increase in the phase speed of the Rayleigh wave is observed with the increase in water content in the pores. With the increase in water, the bulk modulus and the density of fluid mixture increase in the medium. This enhances the phase speed of P-wave and in turn, increases the phase speed of the Rayleigh surface wave traveling on the boundary of the medium. The variation in attenuation coefficient is in accordance with the observed behavior of phase speed in all the cases in the frequency range under consideration.

The variation in phase speed and the attenuation coefficient of the Rayleigh wave in both the composites at different values of porosity are depicted in figures 5-6. The sand fraction (S_{s_2}) and water saturation (S_2) in this case are fixed at 0.5. It is observed that an increase in porosity slows down the Rayleigh wave in both systems. The increase in the porosity of a medium decreases the shear modulus of the medium and in turn decreases the phase speed of the Rayleigh wave.

Figure 7 depicts the particle motion for Rayleigh surface wave propagating on composite porous medium saturated by oil and water at different depths with different porosities. As expected, the particle traces an elliptical curve during the propagation of the wave. Also, the horizontal and vertical displacements of the particle decay with depth. The rate at which the displacement decays increases with the depth. With an increase in the porosity

of a medium, amplitudes of the particle motion decrease sharply. A small tilt in the polarization of the particle motion is also observed. It means that porosity changes the orientation of an elliptical motion of the particle during the propagation of the Rayleigh surface wave. It is observed that the Van Genuchten (VG) parameters $\mathfrak{g}$, $\mathfrak{h}$ and $\mathfrak{i}$ given in Appendix play important role. The parameters $\mathfrak{g}$ and $\mathfrak{h}$ signifies the shape parameters of soil-water characteristic, whereas the fitting parameter $\mathfrak{i}$ corresponds to scale parameter, which is inversely proportional to mean pore diameter. Yang and You (2013) have defined a range in which the values of these parameters lie for different materials. For sand-ice composite the value of $\mathfrak{h}$ is assumed to be 1.16, while for sand-ice it is taken to be 1.29. The value of $\mathfrak{i}$ is assumed to be 0.00015 for both the systems.

6 Conclusion

Present formulation depicts the effect of composite material on Rayleigh surface wave propagating at the stress free boundary of a composite porous matrix containing two immiscible fluids. The Rayleigh wave propagating in the considered medium is similar to the quasi-elastic wave usually propagates in a poroelastic medium. A numerical study is conducted to observe the effect of distinct composite materials on the phase speed of the Rayleigh wave. Based on the numerical study, it may be concluded that an increase in the permeability of the material favors the propagation of the Rayleigh surface wave and hence increases the phase speed of the wave. This fact is based upon the observation that an increase in ice in the sand-ice composite, and a decrease in clay in the sand-clay composite increases the phase speed of the wave. The increase in porosity of the medium decreases the shear modulus and hence decreases the phase speed of the Rayleigh wave significantly. Also, it is noticeable that an increase in fluid density and bulk modulus of the water-oil mixture present in the pores of the composite matrix increases the phase speed of the Rayleigh wave. Increase in porosity of the medium rapidly changes the orientation of the elliptic path of the particles during the propagation of the Rayleigh wave in the medium. The results obtained are significant for non-invasive geotechnical

characterization and subsurface hydrology. The study is also helpful in analyzing the properties of reinforced composite materials.

Appendix

(a) Expressions of coefficients appearing due to inertial and viscous drag:

$A_{11} = S_{s_1}(\rho_1\theta_1 - q_1\phi^2),\ A_{22} = S_{s_1}(\rho_2\theta_2 - q_2\phi^2),\ B_{11} = S_{s_2}(\rho_1\theta_1 - q_1{}'\phi^2),$
$B_{22} = S_{s_2}(\rho_2\theta_2 - q_2{}'\phi^2), A_{12} = -0.1\sqrt{q_1q_2{}'},\ R_{11} = \dfrac{-\theta_1^2\eta_1}{\mathbb{K}_s\mathbb{K}_{r1}},\ \ R_{22} = \dfrac{-\theta_2^2\eta_2}{\mathbb{K}_s\mathbb{K}_{r2}},$
$R_{12} = 0, q_\gamma = \dfrac{T_{s_1}\rho_\gamma S_\gamma}{\phi},\ q_\gamma{}' = \dfrac{T_{s_2}\rho_\gamma S_\gamma}{\phi}, \mathbb{K}_s = S_{s_1}\mathbb{K}_{s_1} + S_{s_2}\mathbb{K}_{s_2},$
$\mathbb{K}_{r1}(S_2) = (1-S_2)^\eta[1-(S_2)^{\frac{1}{\mathfrak{g}}}]^{2\mathfrak{g}}, \mathbb{K}_{r2}(S_2) = (S_2)^\eta[(1-(1-(S_2)^{\frac{1}{\mathfrak{g}}}))^{\mathfrak{g}}]^2,$
$\dfrac{dp_c}{dS_1} = \dfrac{1}{\mathfrak{g}\mathfrak{h}\mathfrak{i}}[(1-S_1)^{\frac{-\mathfrak{h}}{\mathfrak{h}-1}} - 1]^{\frac{1-\mathfrak{h}}{\mathfrak{h}}}(1-S_1)^{\frac{-(2\mathfrak{h}-1)}{\mathfrak{h}-1}},$

where K_α represents bulk modulus of each phase. $\mathbb{K}_{s_1}$ and $\mathbb{K}_{s_2}$ represent permeability of first and second solid, respectively where as η_γ corresponds to viscosity of fluid phases. The symbols T_{s_γ} corresponds to the tortuosity of the solids, which depends upon porosity (ϕ). For numerical purpose their values are obtained from the relation $T_{s_\gamma} = \dfrac{1}{2}(1 + \dfrac{1}{\phi})$. The symbols $S_\gamma = \dfrac{\theta_\gamma}{\phi}$ and $S_{s_\gamma} = \dfrac{\theta_{s_\gamma}}{\theta_s}$, $\quad(\theta_s = \theta_{s_1} + \theta_{s_2})$ correspond to saturation of fluid phases and solid fraction in composite matrix, respectively. Pore space is considered to be completely filled by fluids. Mathematically, this can be written as $S_1 + S_2 = 1$. Dry bulk modulus of each solid is depicted by $K^d_{s_\gamma}$. The term p_c signifies the pressure difference between fluid phases. The symbols $\mathfrak{h}$, and $\mathfrak{g} = 1 - \frac{1}{\mathfrak{h}}$ correspond to VG fitting parameters. The value of the fitting parameter η is taken to be 0.45. For numerical discussion we have considered $\mathfrak{h} = 1.16$ for Sand-Ice composite and 1.36 for Sand-Clay composite system.

(b) Expressions of coefficients appearing in stress strain relation:

$a_{11} = K_{s_1}S_{s_1}(-\delta_{s_1} + \theta_s),\ \ a_{12} = -K_{s_1}S_{s_1}\delta_1,$
$a_{13} = -K_{s_1}S_{s_1}\delta_2,\ \ a_{34} = -K_{s_2}S_{s_2}\delta_2, a_{14} = -K_{s_1}S_{s_1}\delta_{s_2} = -K_{s_2}S_{s_2}\delta_{s_1},$
$a_{22} = \dfrac{-1}{M_1}\Big[M_3\delta_1 + \dfrac{K_1K_2S_1\phi}{1-S_1}\dfrac{dS_1}{dp_c} + K_1\phi S_1\Big],$
$a_{23} = \dfrac{-1}{M_1}\Big[\dfrac{\delta_1\delta_2M_1(K_{s_1}S_{s_1} + K_{s_2}S_{s_2})}{\delta_{s_1} + \delta_{s_2}} + K_1K_2\phi\dfrac{dS_1}{dp_c}\Big],\ \ a_{24} = -K_{s_2}S_{s_2}\delta_1,$
$a_{33} = \dfrac{-1}{M_1}\Big[M_4\delta_2 + \dfrac{K_1K_2(1-S_1)\phi}{S_1}\dfrac{dS_1}{dp_c} + K_2(1-S_1)\phi\Big],\ \ a_{44} = K_{s_2}S_{s_2}(-\delta_{s_2} + \theta_s),$

$$\delta_1 = \frac{M_3}{M_1\left(K_{s_1}S_{s_1}+K_{s_2}S_{s_2}\right)}\left(\delta_{s_1}+\delta_{s_2}\right), \quad M_1 = -\left(1+\frac{K_2}{1-S_1}\frac{dS_1}{dp_c}+\frac{K_1}{S_1}\frac{dS_1}{dp_c}\right),$$
$$\delta_2 = \frac{M_4}{M_1\left(K_{s_1}S_{s_1}+K_{s_2}S_{s_2}\right)}\left(\delta_{s_1}+\delta_{s_2}\right), \quad M_2 = \frac{K_1K_2}{\phi S_1(1-S_1)}\frac{dS_1}{dp_c}+\frac{K_1S_1}{\phi}+\frac{K_2(1-S_1)}{\phi},$$
$$M_3 = \frac{K_1K_2S_1}{1-S_1}\frac{dS_1}{dp_c}+K_1S_1+K_1K_2\frac{dS_1}{dp_c}, \quad M_4 = K_1K_2\frac{dS_1}{dp_c}+K_2\left(\frac{K_1}{S_1}\frac{dS_1}{dp_c}+1\right)(1-S_1),$$
$$\delta_{s_\gamma} = K_{s_\gamma}\left(\frac{-1}{K_{s_\gamma}}+\frac{\theta_{s_\gamma}}{K^d_{s_\gamma}}\right)\left[\mathcal{B}+\frac{M_2\left(1-\frac{K_{s_\gamma}\theta_{s_\gamma}}{K^d_{s_\gamma}}\right)}{M_1K_{s_\gamma}S_{s_\gamma}}\right]^{-1}, \mathcal{B} = \left(\frac{K_{s_1}\theta_{s_1}}{K^d_{s_1}}+\frac{K_{s_2}\theta_{s_2}}{K^d_{s_2}}\right)\frac{1}{1-\phi}.$$

(c) Expressions of coupling coefficients:

ℓ_1=$Det[X_4\ X_2\ X_3]$, ℓ_2=$Det[X_1\ X_4\ X_3]$, ℓ_3=$Det[X_1\ X_2\ X_4]$, ℓ_4=$Det[X_1\ X_2\ X_3]$,

ϵ_1=$Det[X_8\ X_6\ X_7]$, ϵ_2=$Det[X_5\ X_8\ X_7]$, ϵ_3=$Det[X_5\ X_6\ X_8]$, ϵ_4=$Det[X_5\ X_6\ X_7]$,

where Det is employed to symbolize the determinant of a matrix. Also,

$X_1 = [a_{22}\mathrm{Y}+\eta_{11}\ \ a_{23}\mathrm{Y}+\eta_{12}\ \ a_{24}\mathrm{Y}+\eta_{01}]^T$, $X_2 = [a_{23}\mathrm{Y}+\eta_{12}\ \ a_{33}\mathrm{Y}+\eta_{23}\ \ a_{34}\mathrm{Y}+\eta_{02}]^T$,

$X_3 = [a_{24}\mathrm{Y}+\eta_{01}\ \ a_{34}\mathrm{Y}+\eta_{02}\ \ a_{44}^{-}\mathrm{Y}+\eta_{44}]^T$, $X_4 = -[a_{12}\mathrm{Y}+\eta_{01}\ \ a_{13}\mathrm{Y}+\eta_{02}\ \ a_{14}\mathrm{Y}+\eta_{03}]^T$,

$X_5 = [\eta_{11}\ \ \eta_{12}\ \ \eta_{01}]^T$, $X_6 = [\eta_{12}\ \ \eta_{23}\ \ \eta_{02}]^T$, $X_7 = [\eta_{01}\ \ \eta_{02}\ \ G_{s_2}\mathrm{Y}+\eta_{44}]^T$,

$X_8 = -[\eta_{01}\ \ \eta_{02}\ \ \eta_{03}]^T$,

$$\lambda^\beta_{s_1} = 1,\ \lambda^\beta_1 = \frac{\ell_1}{\ell_4},\ \ \lambda^\beta_2 = \frac{\ell_2}{\ell_4},\quad \lambda^\beta_{s_2} = \frac{\ell_3}{\ell_4},\qquad \mathrm{Y} = \frac{-1}{v^2_\beta},$$
$$\lambda^l_{s_1} = 1,\ \lambda^l_1 = \frac{\epsilon_1}{\epsilon_4},\ \ \lambda^l_2 = \frac{\epsilon_2}{\epsilon_4},\quad \lambda^l_{s_2} = \frac{\epsilon_3}{\epsilon_4},\qquad \mathrm{Y} = \frac{-1}{v^2_l}.$$

where v_β, v_l correspond to phase speed of four dilatational and two shear waves, respectively.

References

Albers, B., On results of the surface wave analyses in poroelastic media by means of the simple mixture model and the Biot model, Soil Dyn Earthq Eng., vol. **26** pp. 537-547, 2006. DOI: 10.1016/j.soildyn.2006.01.007

Arora, A., Painuley, A. and Tomar, S. K., Body waves in composite solid matrix containing two immiscible fluids, Transp Porous Med., vol. **108**, pp. 531–554, 2015. DOI: 10.1007/s11242-015-0486-9

Arora, A., Bala, N. and Tomar, S. K., A mathematical model for wave propagation in a composite solid matrix containing two immiscible fluids, Acta Mech., vol. **227**, pp. 1453

-1467, 2016. DOI: 10.1007/s00707-016-1571-z

Borcherdt, R. D., Rayleigh-type surface wave on a linear viscoelastic half-space, J Acoust Soc Am., vol. **54**, no. 6, pp. 651-1653, 1973.

Carcione, J. M., Rayleigh waves in isotropic viscoelastic media, Geophys J Int., vol. **108**, no. 2, pp. 453-464, 1992. DOI: 10.1111/j.1365-246X.1992.tb04628.x

Colombi, A., Roux. P., Colquitt, D. J., Guenneau, S., Ageeva, V., Clark, M. and Craster, R., New frontiers in elastic metamaterials for controlling surface waves, J Acoust Soc Am., vol. **140**, no. 4, pp. 3103-3103, 2016. DOI: 10.1121/1.4969683

Currie, P. K., Hayes, M. A. and O'Leary, P. M., Viscoelastic Rayleigh waves, Q Appl Math., vol. **35**, no. 1, pp. 35-53, 1977.

Currie, P. K. and O'Leary, P. M., Viscoelastic Rayleigh waves II., Q Appl Math., vol. **36**, pp. 445-454, 1978.

Currie, P. K., Viscoelastic surface waves on a standard linear solid, Q Appl Math., vol **37**, no. 3, pp. 332-336, 1979.

Dai, Z., Kuang, Z. and Zhao, S., Rayleigh waves in a double porosity half-space, J Sound Vib., vol. **298**, pp. 319-332, 2006. DOI: 10.1016/j.jsv.2006.05.035

Deresiewicz, H., The effect of boundaries on wave propagation in a liquid-filled porous solid-IV. Surface waves in a half-space, Bull Seismol Soc Am., vol. **52**, no. 3, pp. 627-638, 1962.

Ebrahimi, F. (Ed.), Surface waves: New trends and developments, London: IntechOpen, 2018. DOI: 10.5772/intechopen.68840

Ewing, W. M. and Jardetzky, W. S., Elastic waves in layered media, New York: Frank Press, McgrawHill, 1957.

Foti, S., Lai, C. G., Rix, G. J. and Strobbia, C., Surface wave methods for near surface site characterization, New York: CRC Press, Taylor & Francis Group, 2015. DOI: 10.1201/b17268

Gupta, S. and Ahmed, M., Influence of prestress and periodic corrugated boundary surfaces on Rayleigh waves in an orthotropic medium over a transversely isotropic dissipative semi infinite substrate, The Eur. Phys. J Plus., vol. **132**, no. 8, 2017. DOI:

10.1140/epjp/i2017-11282-6

Jones, J. P., Rayleigh waves in a porous, elastic, saturated solid, J Acoust Soc Am., vol. **33**, no. 7, pp. 959-962, 1961.

Kumari, A., Kundu, S. and Gupta, S., Propagation and attenuation characteristics of Rayleigh waves induced due to irregular surface in liquid-saturated micropolar porous half-space, Eur. Phys. J. Plus., vol. **134**, pp. 576, 2019. DOI: 10.1140/epjp/i2019-12839-y.

Leclaire, P., Cohen-Tenoudji, F. and Aguirre-Puente, J., Extension of Biot's theory of wave propagation to frozen porous media, J Acoust Soc Am., vol. **96**, pp. 3753-3768, 1994. DOI: 10.1121/1.411336

Lo, W. C., Sposito, G. and Majer, E., Wave propagation through elastic porous media containing two immiscible fluids, Water Resour Re., vol. **41**, pp. 1-20, 2005. DOI: 10.1029/2004WR003162

Lo, W. C., Propagation and attenuation of Rayleigh waves in a semi-infinite unsaturated poroelastic medium, Adv Water Resour, vol. **31**, no. 10, pp. 1399-1410, 2008. DOI: 10.1016/j.advwatres.2008.07.008

Moro, G. D., Surface Wave Analysis for Near Surface Applications, Amsterdam: Elsevier, 2015. DOI: 10.1016/C2013-0-18480-2

Nenadic, I. Z., Urban, M. W., Bernal, M. and Greenleaf, J. F., Phase velocities and attenuations of shear, Lamb, and Rayleigh waves in plate-like tissues submerged in a fluid (L), J Acoust Soc Am, vol. **130**, no. 6, PP. 3549, 2011. DOI: 10.1121/1.3654029

Omrani, H., Hassini, L., Benazzouk, A., Beji, H. and ELCafsi, A., Elaboration and characterization of clay-sand composite based on Juncus acutus fibers, Const Build Mat., vol.**238**, 117712, 2020. DOI: 10.1016/j.conbuildmat.2019.117712

Painuley, A. and Arora, A., Rayleigh wave at composite porous half space saturated by two immiscible fluids, Appl Math Model., vol. **73**, pp. 124-135, 2019. DOI: 10.1016/j.apm.2019.03.038

Romeo, M., Rayleigh Waves on a Viscoelastic Solid Half-Space, J. Acous. Soc. Am., vol. **110**, pp. 59-67, 2001.

Sharma, M. D., Rayleigh waves in a partially saturated poroelastic solid, Geophys J Int.,

vol. **189**, no. 2, pp. 1203-1214, 2012, DOI: 10.1111/j.1365-246X.2012.05433.x

Sharma, M. D., Propagation of Rayleigh waves at the boundary of an orthotropic elastic solid: Influence of initial stress and gravity, J Vib Cont. DOI: 10.1177/1077546320912069

Singh, P., Chattopadhyay, A. and Singh, A. K., Rayleigh-type wave propagation in incompressible visco-elastic media under initial stress, App Math and Mech., vol. **39**, pp. 317–334, 2018. DOI: 10.1007/s10483-018-2306-9

Vasiliev, N., Pronk, A. D. C., Shatalina, I.N. and Janssen, F. H. M. E., A Review on the Development of Reinforced Ice for Use as a Building Material in Cold Regions, Cold Reg Sc Tech., Vol. **115**, 2015. DOI: 115. 10.1016/j.coldregions.2015.03.006

Vinh, P. C., Aoudia, A. and Giang, P. T. H., Rayleigh waves in orthotropic fluid-saturated porous media, Wave Motion., vol. **61**. pp. 73-82, 2016. DOI: 10.1016/j.wavemoti.2015.10.007

Yang. Xu., You. Xueyi., Estimating parameters of Van Genuchten model for soil water retention curve by intelligent algorithm, Appl. Math. Inf. Sc. vol. **7** no. 5, 1977-1983, 2013.

Yilmaz, Ö. z., Engineering Seismology with Applications to Geotechnical Engineering, Society of exploration geophysicists, Tulsa, 2015. DOI: 10.1190/1.9781560803300

Table-II.

Nomenclature	
ρ_α	density for the phase $\alpha \quad (\alpha = s_1, 1, 2, s_2)$
θ_α	volume fraction for the phase α
σ^α	components of stress on the phase α
$\boldsymbol{u_\alpha}$	displacement field of each phase α
S_γ	saturation of each fluid phase $\quad (\gamma = 1, 2)$
S_{s_γ}	fraction of each solid in composite matrix
R_{11}, R_{22}	coefficients related to viscous drag
A_{11}, A_{22}	coefficients related to inertial drag of first solid
B_{11}, B_{22}	coefficients related to inertial drag of second solid
A_{12}	inertial coupling parameter connecting fluid phases
G_{s_γ}	shear modulus of each solid phase
ω	angular frequency
η_γ	viscosity of fluid phase
P_β	Four dilatational waves in medium $\beta \quad (\beta = 1, 2, 3, 4)$
S_l	Two shear waves in medium $\quad (l = 5, 6)$
k_β	complex wave number of dilatational wave
k_l	complex wave number of rotational wave
k_r	complex wave number of Rayleigh wave
V_r	phase speed of Rayleigh wave
A_r	attenuation coefficient of Rayleigh wave
v_β	phase speed of dilatational wave
v_l	phase speed of rotational wave
K_α	Bulk modulus of α phase
$K^d_{s_\gamma}$	Drained bulk modulus of solid
$\mathbb{K}_{s_\gamma}$	Permeability of solid phase
T_{s_γ}	tortuosity of solid
$\mathbb{K}_{r_\gamma}$	Relative permeability of fluids
ϕ	porosity of medium
p_c	capillary pressure difference between fluids
$\mathfrak{h}$, $\mathfrak{i}$, η	fitting parameters

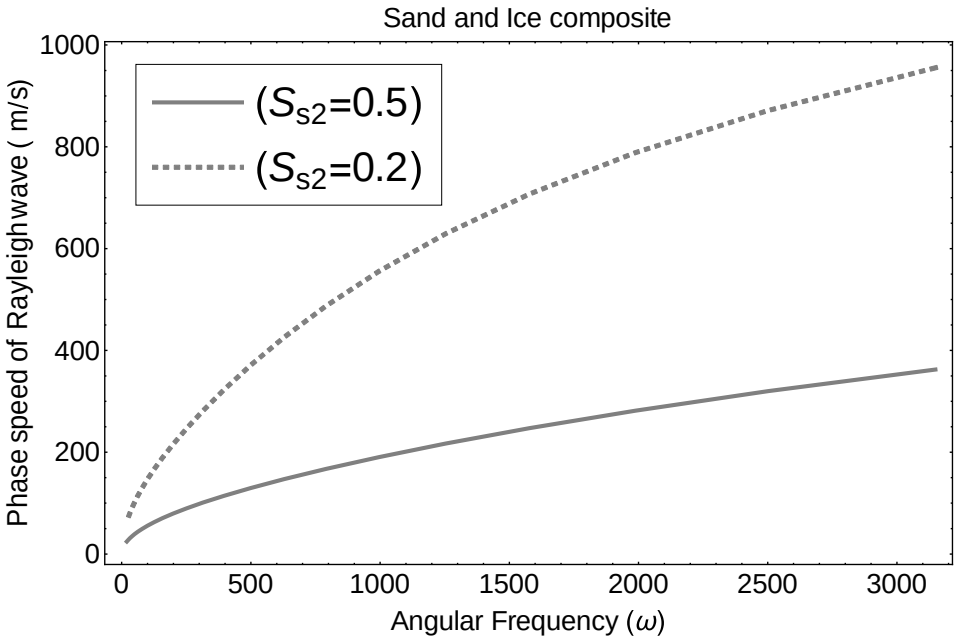

(a)

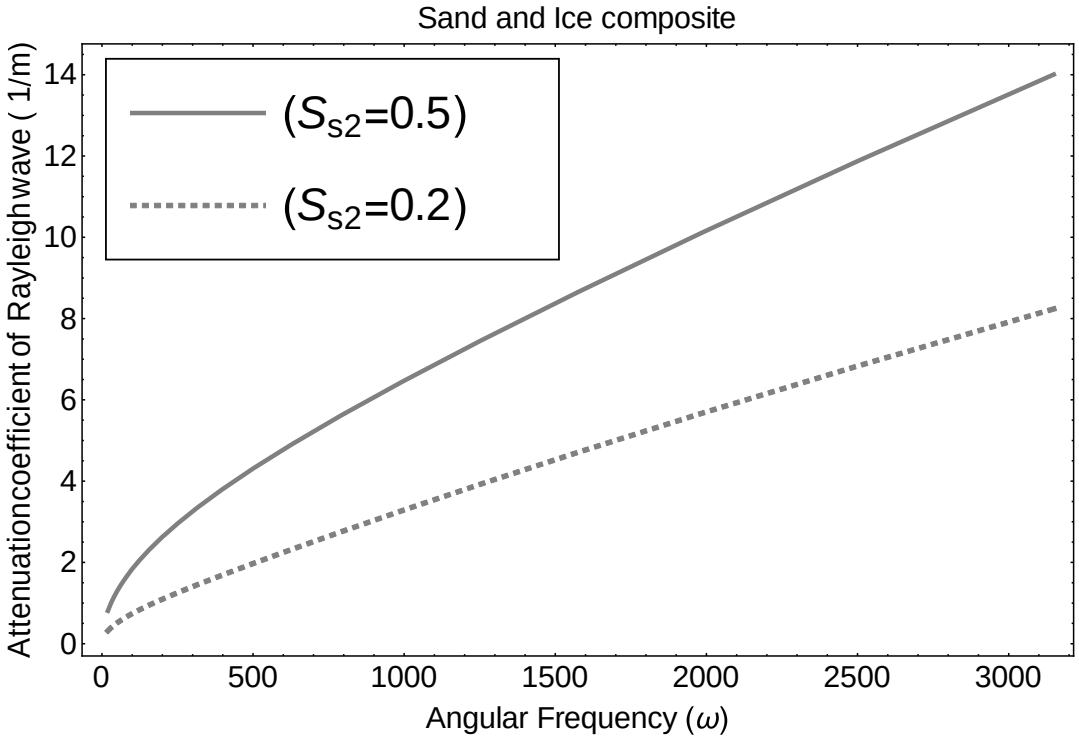

(b)

Figure 1: The variation of phase speed and attenuation coefficient of

Rayleigh wave with angular frequency of Sand-Ice Composite at different fractions of sand.

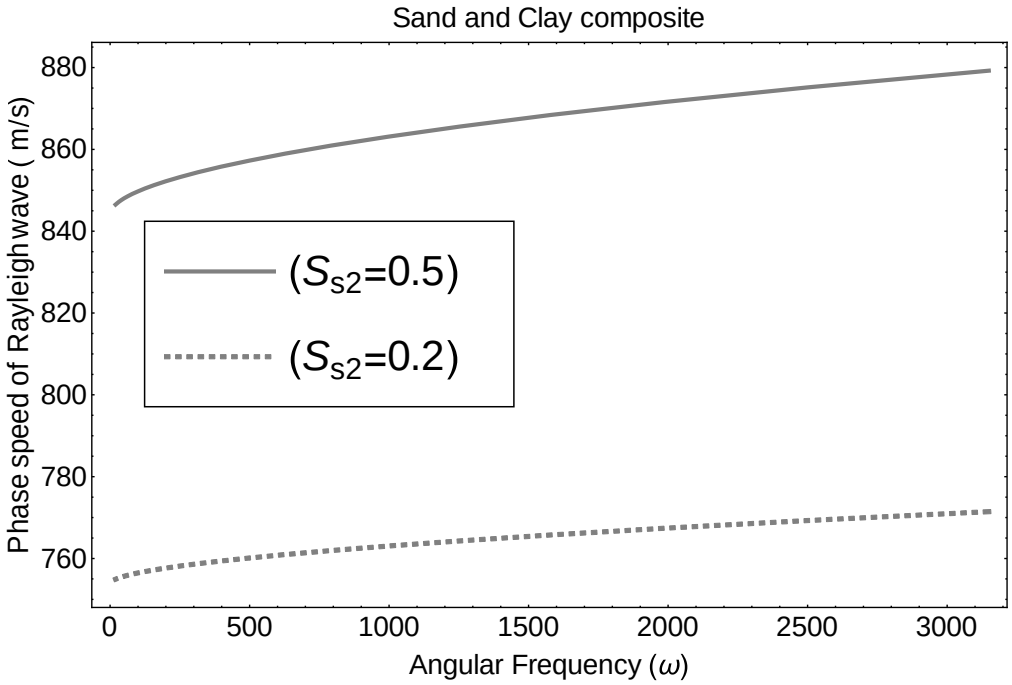

(a)

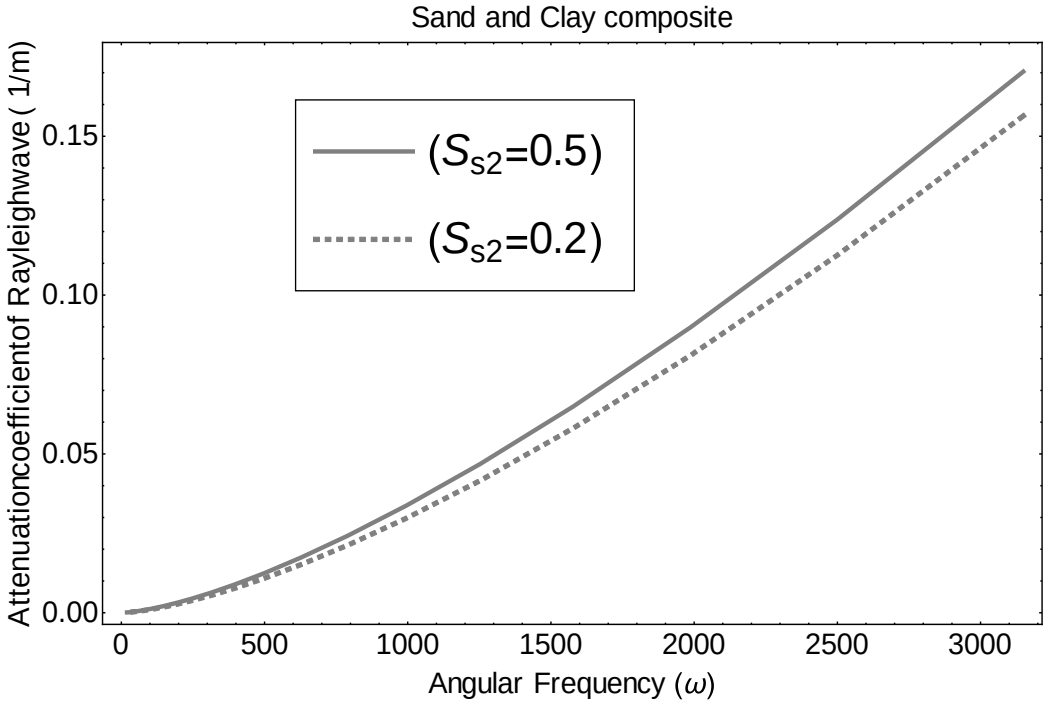

(b)

Figure 2: The variation of phase speed and attenuation coefficient of Rayleigh wave with angular frequency of Sand-Clay composite at different fractions of sand.

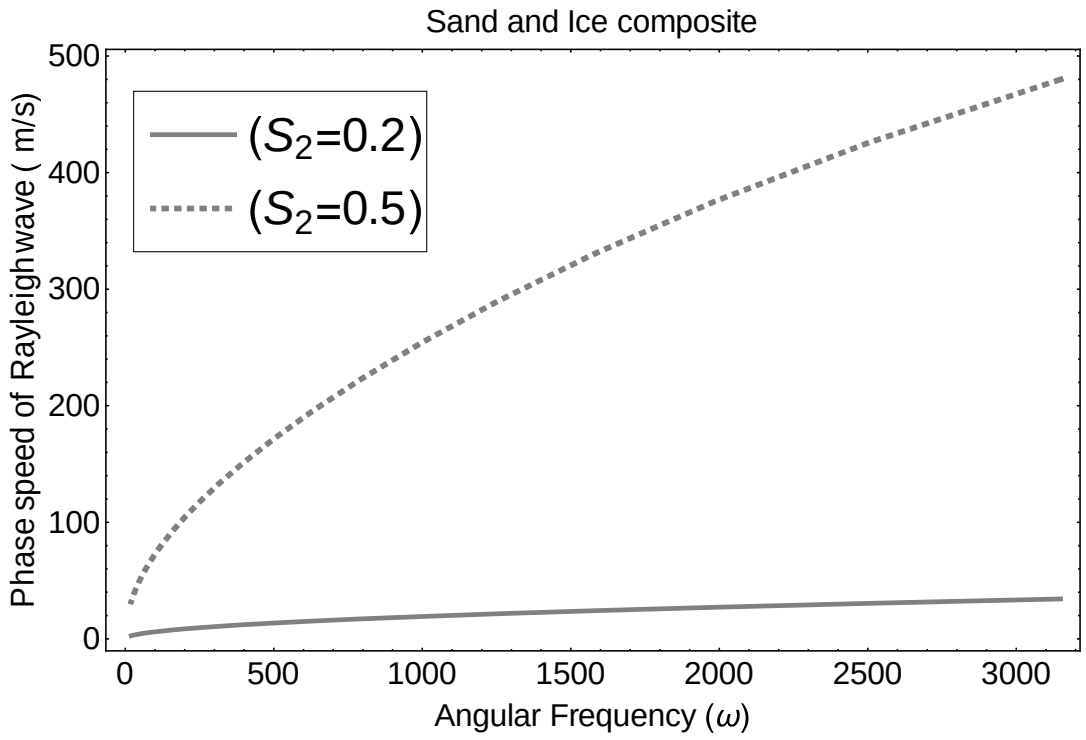

(a)

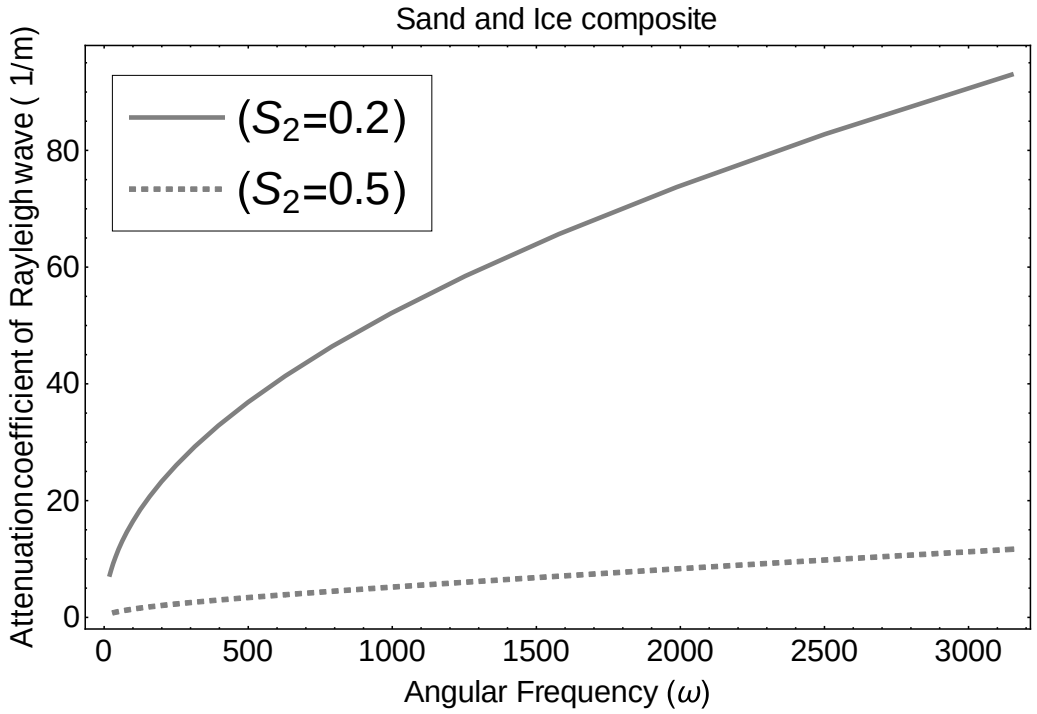

(b)

Figure 3: The variation of phase speed and attenuation coefficient of Rayleigh wave with angular frequency of Sand-Ice Composite at different water saturation.

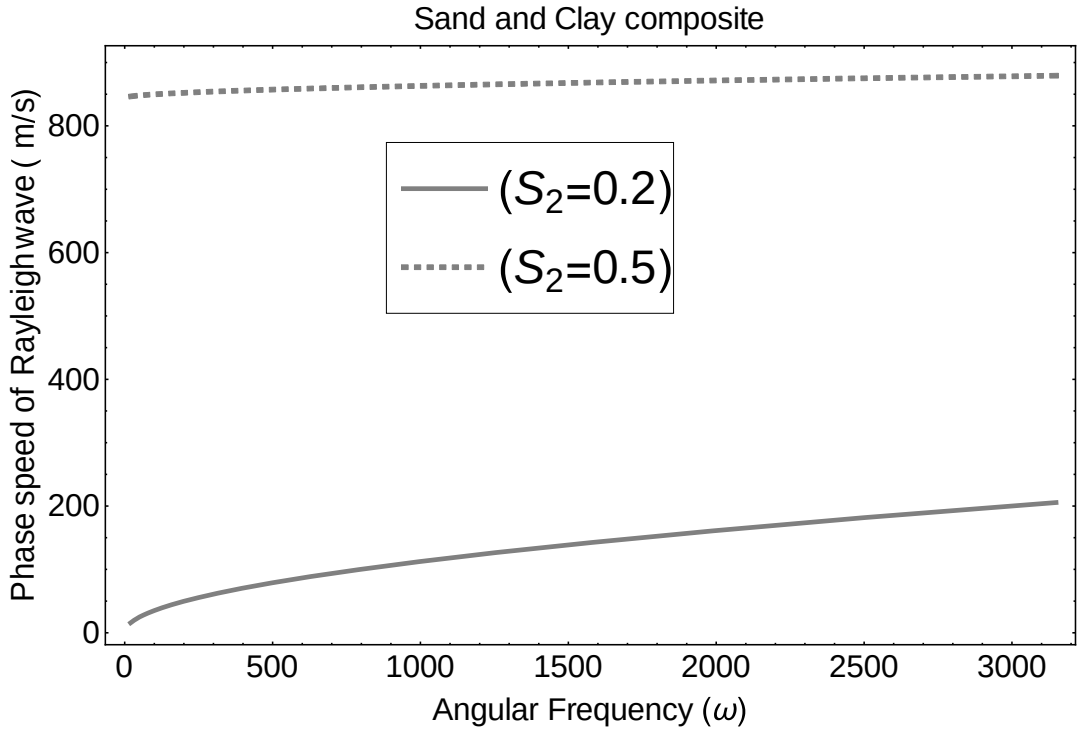

(a)

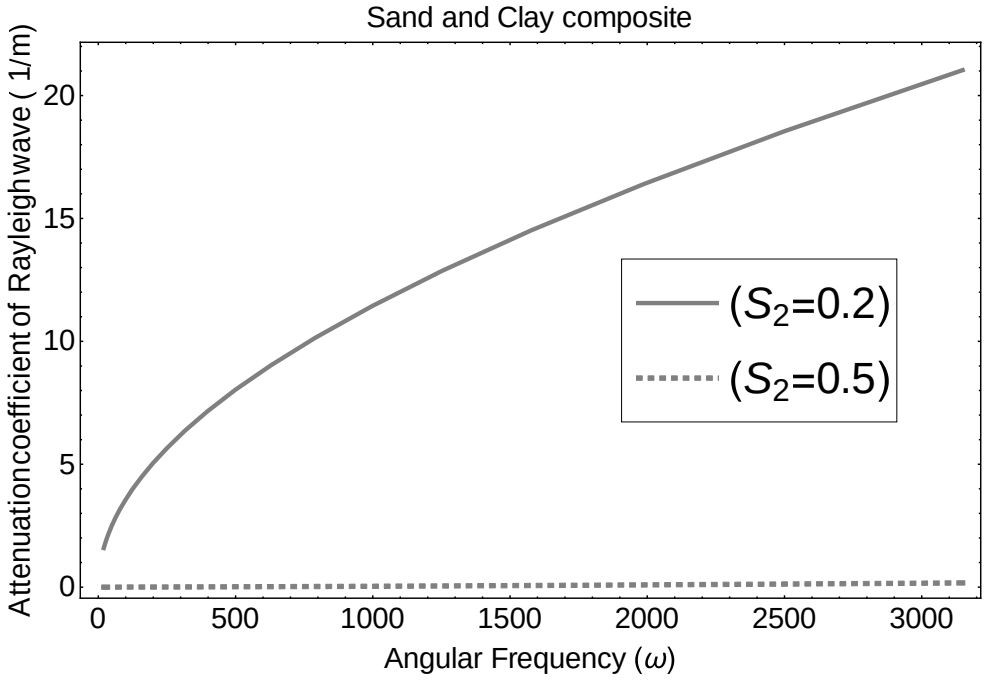

(b)

Figure 4: The variation of phase speed and attenuation coefficient of Rayleigh wave with angular frequency of Sand-Clay Composite at

different water saturation.

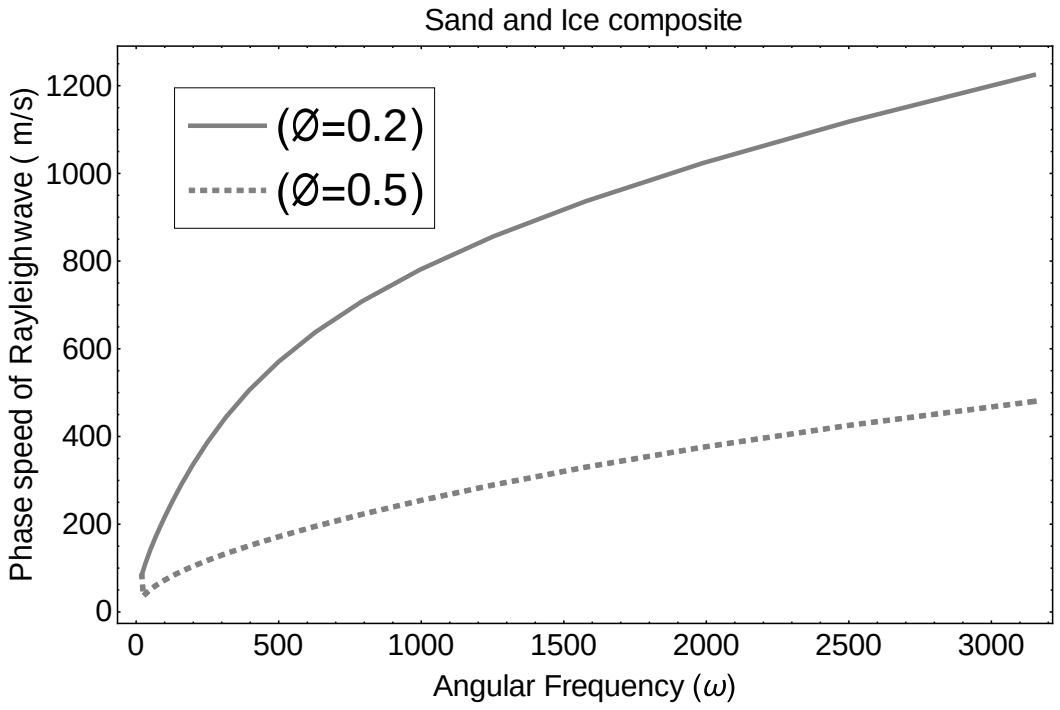

(a)

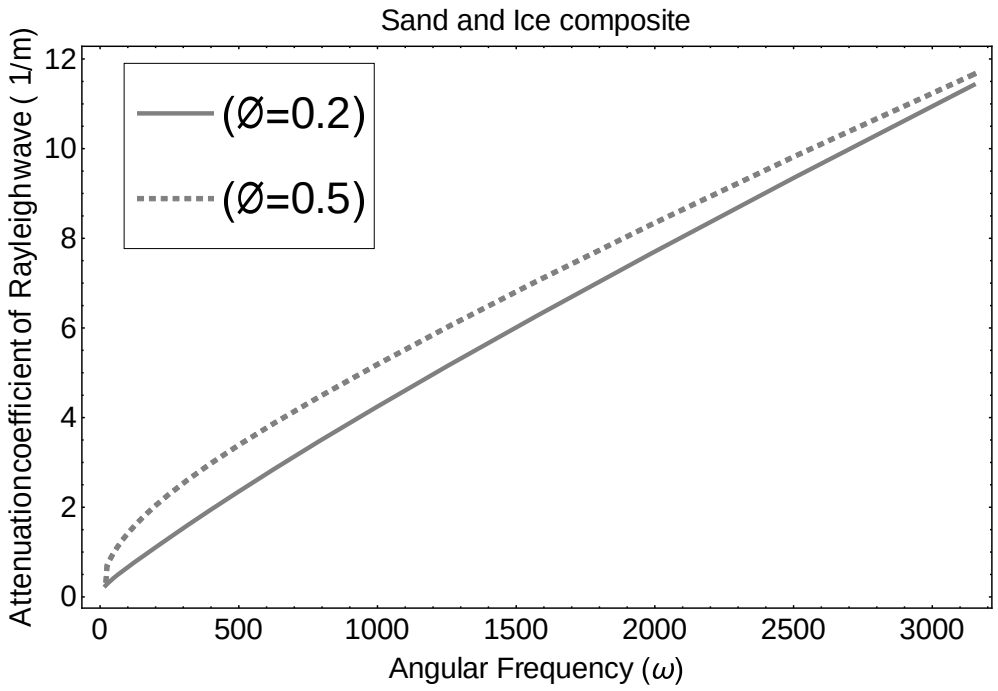

(b)

Figure 5: The variation of phase speed and attenuation coefficient of Rayleigh wave with angular frequency of Sand-Ice Composite at different porosity of medium.

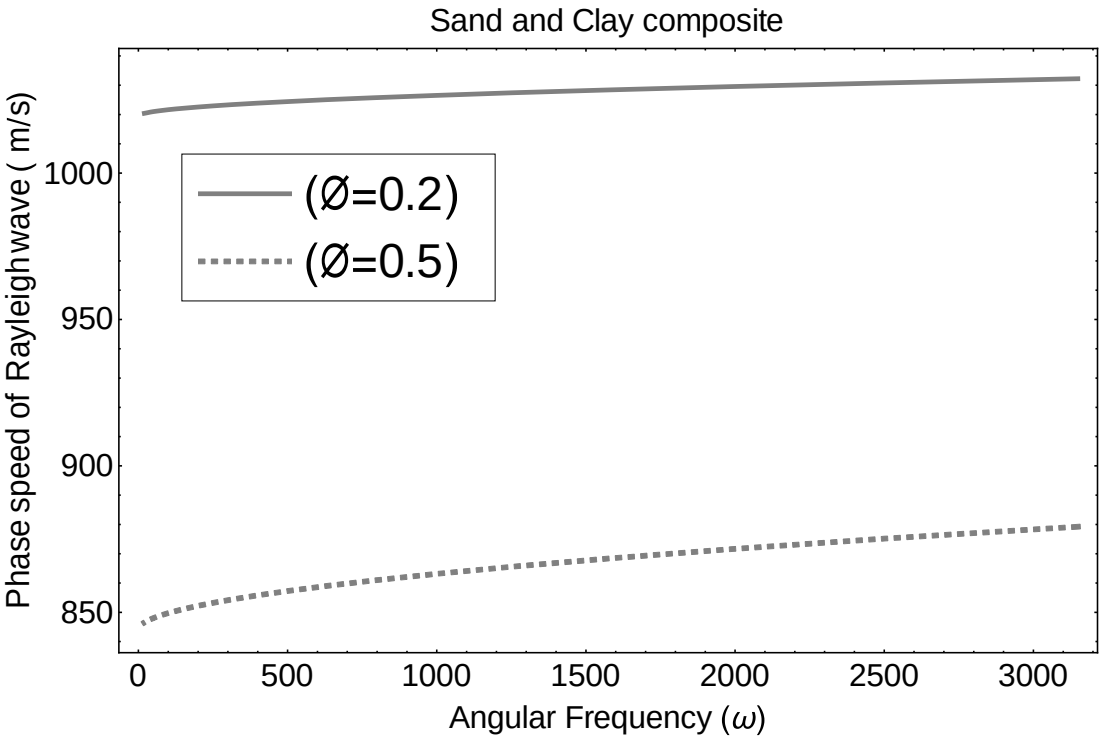
Sand and Clay composite
Phase speed of Rayleighwave (m/s)
1000
950
900
850
(Ø=0.2)
(Ø=0.5)
0
500
1000
1500
2000
2500
3000
Angular Frequency (ω)

(a)

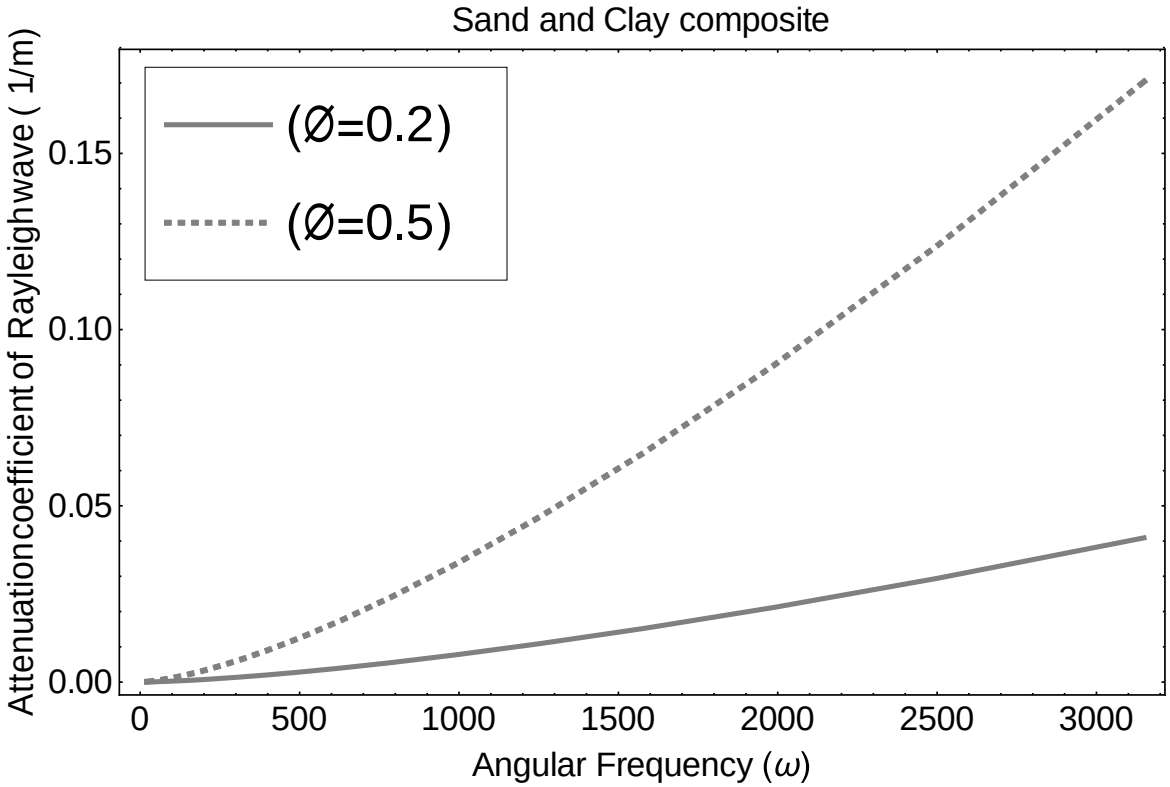
Sand and Clay composite
Attenuationcoefficient of Rayleighwave (1/m)
0.15
0.10
0.05
0.00
(Ø=0.2)
(Ø=0.5)
0
500
1000
1500
2000
2500
3000
Angular Frequency (ω)

(b)

Figure 6: The variation of phase speed and attenuation coefficient of Rayleigh wave with angular frequency of Sand-Clay Composite at different porosity of medium.

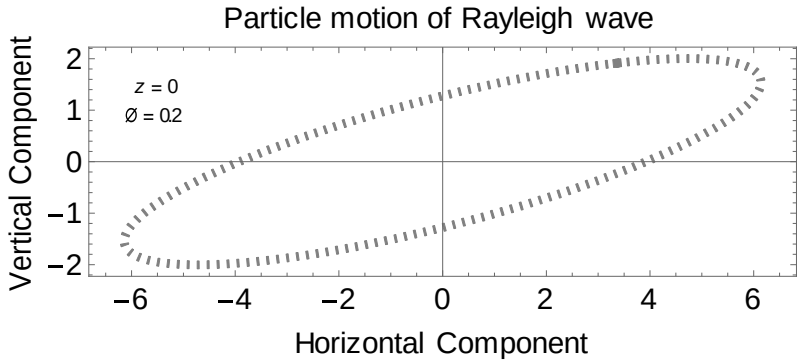

(a)

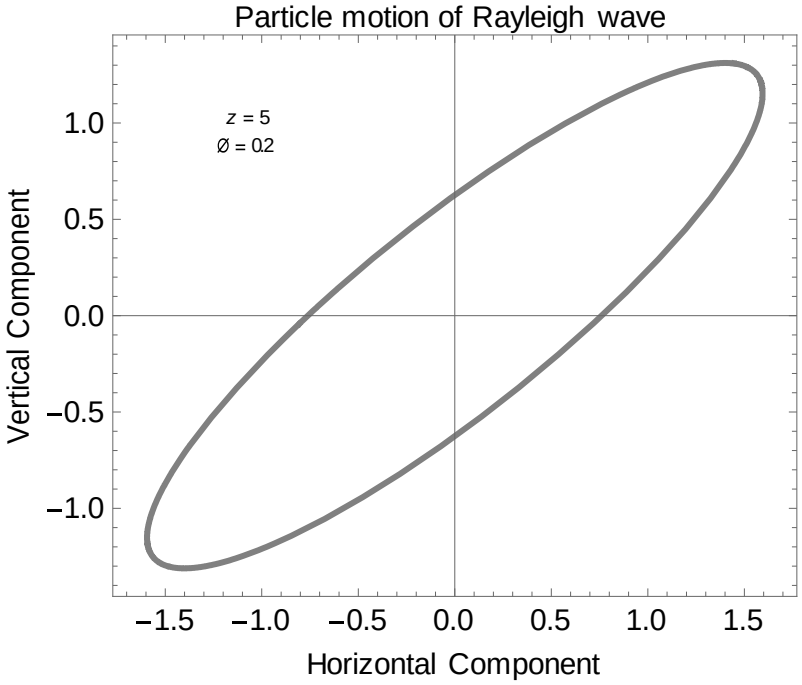

(b)

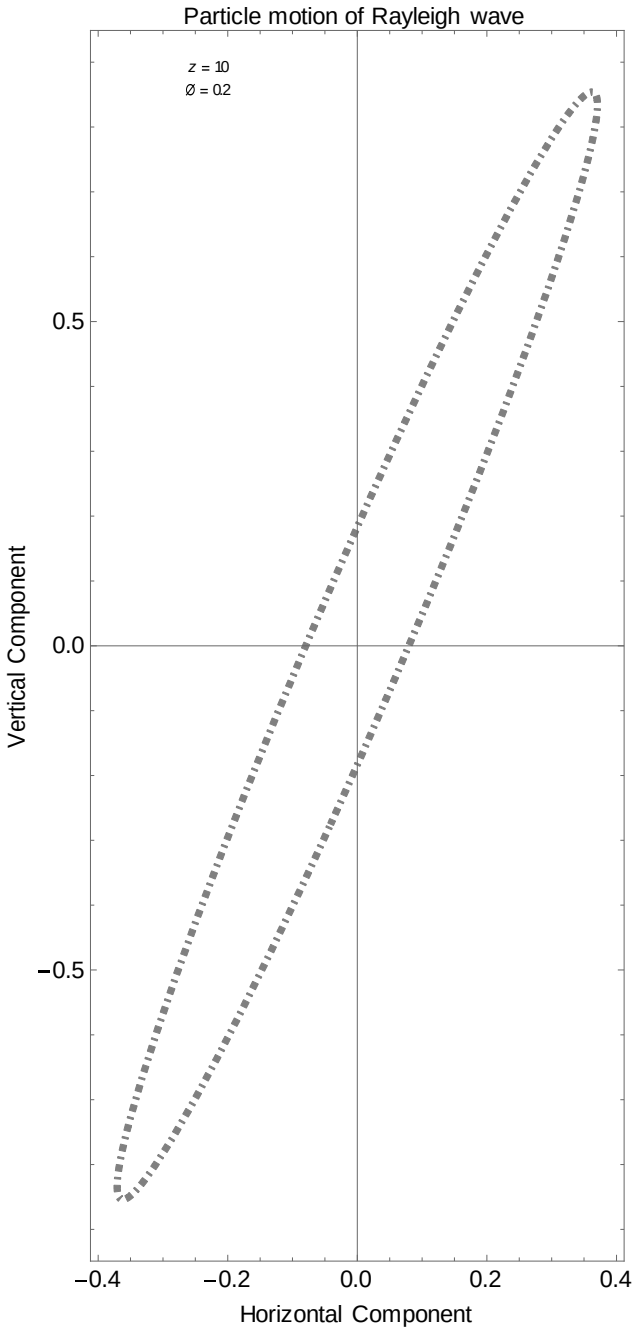
Particle motion of Rayleigh wave
z = 10
Ø = 0.2
0.5
0.0
−0.5
Vertical Component
−0.4
−0.2
0.0
0.2
0.4
Horizontal Component

(c)

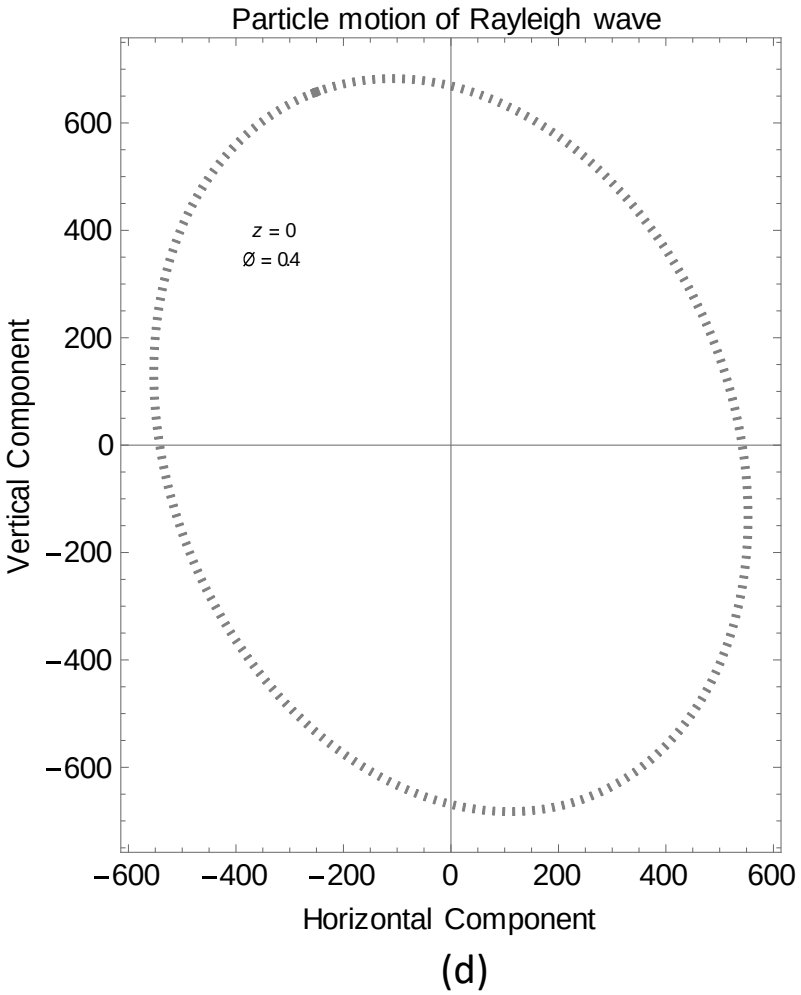
Particle motion of Rayleigh wave
z = 0
Ø = 0.4
600
400
200
0
−200
−400
−600
−600
−400
−200
0
200
400
600
Vertical Component
Horizontal Component

(d)

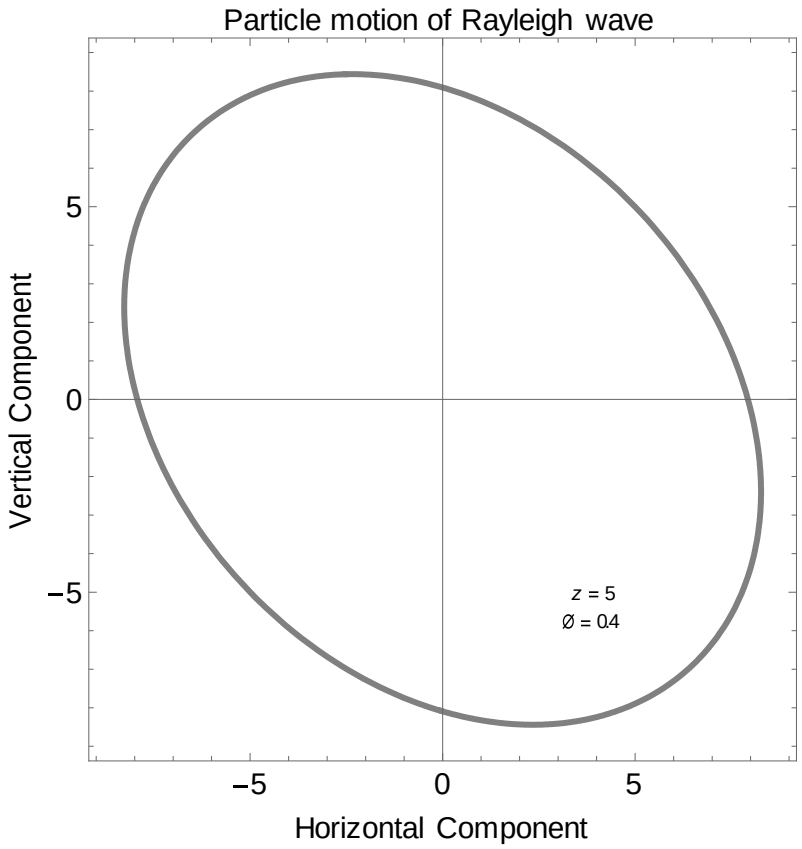
Particle motion of Rayleigh wave
Vertical Component
5
0
−5
−5
0
5
Horizontal Component
z = 5
Ø = 0.4

(e)

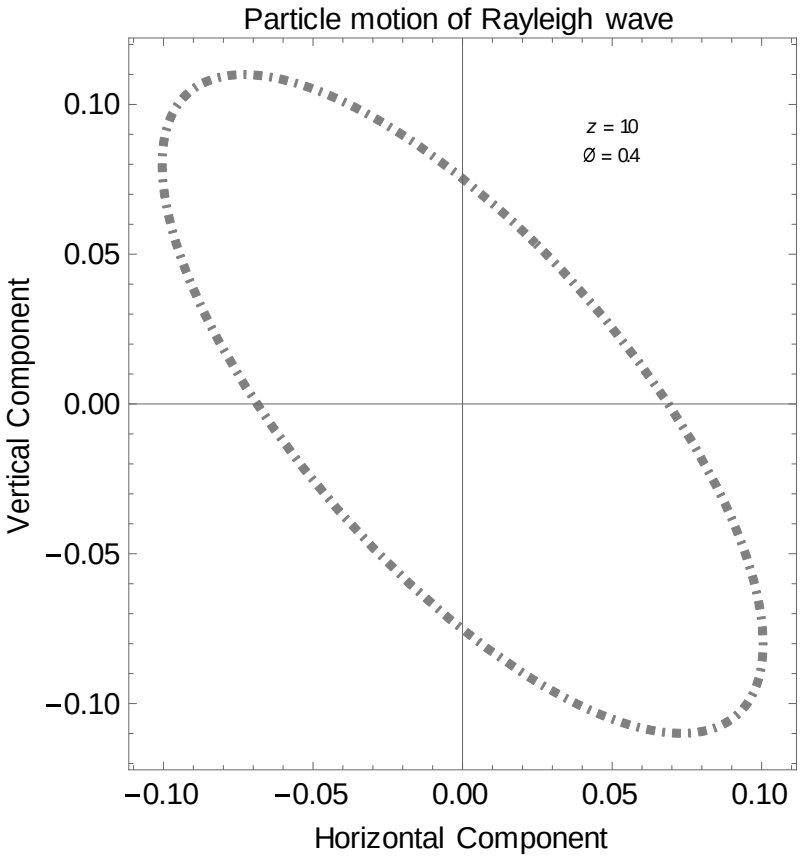
Particle motion of Rayleigh wave
z = 10
Ø = 0.4
0.10
0.05
0.00
−0.05
−0.10
Vertical Component
−0.10
−0.05
0.00
0.05
0.10
Horizontal Component

(f)

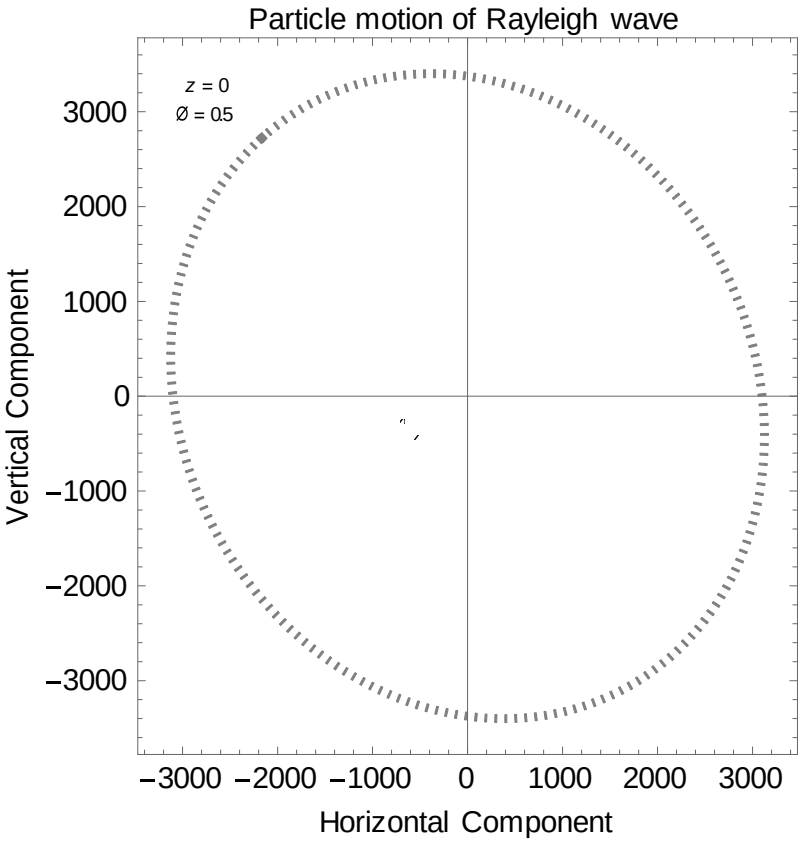
Particle motion of Rayleigh wave
z = 0
Ø = 0.5
3000
2000
1000
0
−1000
−2000
−3000
Vertical Component
−3000 −2000 −1000 0 1000 2000 3000
Horizontal Component

(g)

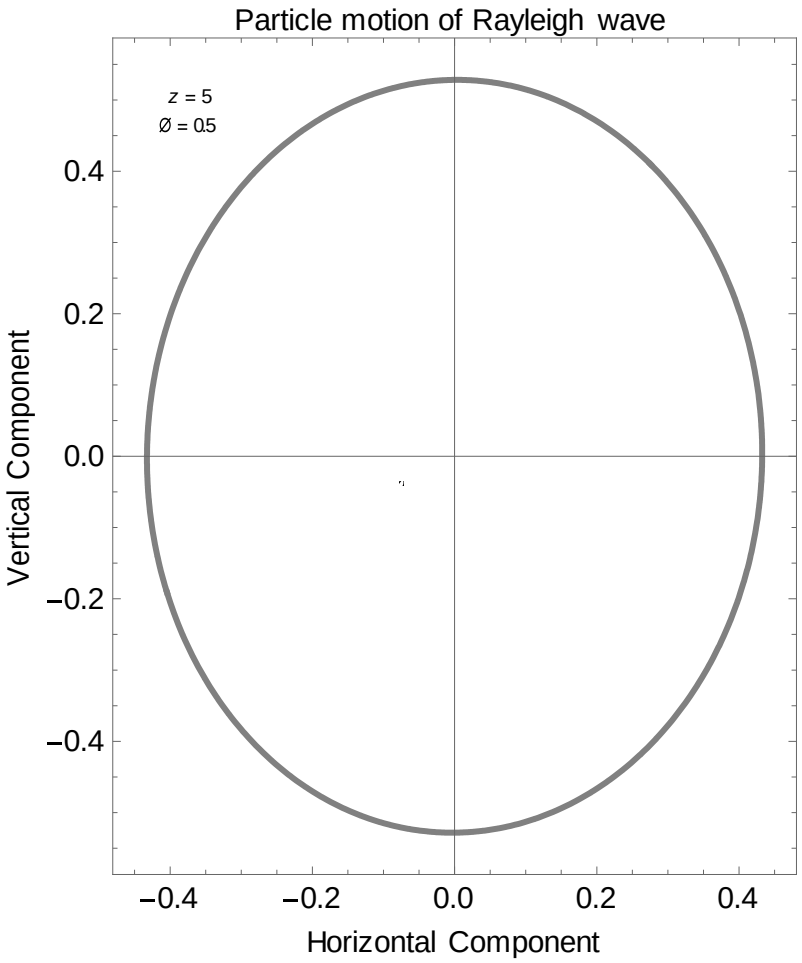
Particle motion of Rayleigh wave
z = 5
Ø = 0.5
0.4
0.2
0.0
−0.2
−0.4
Vertical Component
−0.4
−0.2
0.0
0.2
0.4
Horizontal Component

(h)

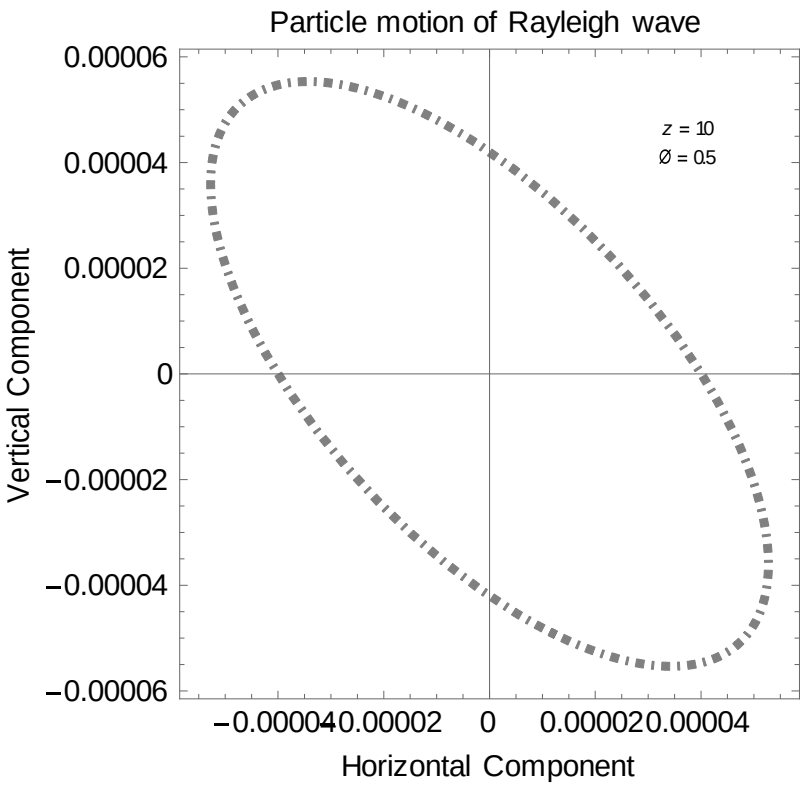

(i)

Figure 7: Particle motion of Rayleigh surface wave at different depths and porosity of a composite porous medium.